

Thermodynamic Model of Ore-forming Processes in a Submarine Island-Arc Hydrothermal System

D. V. Grichuk

Geological Faculty, Moscow State University, Leninskie gory, Moscow, 119991 Russia
e-mail: dgrichuk@yandex.ru

Received April 19, 2012

Abstract—A thermodynamic model suggested for ore-forming processes in a hydrothermal system (HS) in an island arc is based on the technique suggested earlier in [1] for simulating ore-forming hydrothermal systems in mid-oceanic ridges. This technique make use of the principle of flow-through multistep reactor and encompasses (a) the region where hydrothermal solutions are generated when seawater interacts with rocks (descending convection branch); (b) the region where material is transported with the solution at decreasing pressure (feeder channel); and (c) the region where the ore material is deposited (orebody). Hydrothermal systems in island arcs exhibit the following distinctive features taken into account in the model: (1) the composition of the host crustal rocks (rocks of mafic–acid composition instead of basalt and serpentinite) and (2) possible significant involvement of magmatic gases in the feeding of the hydrothermal system. The naturally occurring prototype of the simulated system is the hydrothermal system in the caldera of a submarine volcano in an island arc. The model is simulated in a number of variants in which the hydrothermal fluid is exogenic (heated seawater convecting through hot volcanic rocks), magmatic, or mixed (magmatic plus exogenic) is involved.

The simulations were carried out using the HCh version 4.3 [2] program package for the multisystem H–O–K–Na–Ca–Mg–Fe–Al–Si–C–S–Cl–Cu–Zn–Pb–As–Sb–Ag–Au at temperatures of 25–370°C and pressures of 10–500 bar. The multisystem included 88 possible solid phases and aqueous solution with 95 species. The thermodynamic properties of compounds were calculated using the UNITHERM databank. The model is underlain by the principle of multiwave flow-through multistep reactor (MFTMR) with a starting rock/water (R/W) ratio of 1 : 1. As progressively more solution portions passed through the rocks, the participation of fresh rock in the interaction accordingly diminished because the rock material was gradually exhausted in the system. The magmatic fluid had a composition selected based on data on fumaroles at Kudryavyi volcano [3] with a correction for the degassing pressure. The evolution of ore deposition was simulated in compliance with the scheme described in [4], which was implemented using the technology of “openness from above” [3]. The model was simulated with various compositions of the host rocks (basalts, andesites, dacites, and rhyolites) and the origin of the fluid (magmatic fluid alone, seawater alone, and variable proportions of both).

Our simulation results indicate that the metallogeny (relative enrichment in Pb, As, Sb, or Ag) of island-arc ore deposits is controlled by the abundances of metals in the host rocks predominant in the hydrothermal system. The mineralogy and geochemistry of ores generated in arc hydrothermal systems are predetermined by the effective transport of metalloids (S, As, and Sb) that have a high migration capacity in these systems. Magmatic gases introduced in the hydrothermal systems play dualistic roles in the ore-forming processes. If the hydrothermal fluid in a hydrothermal system is dominated by magmatic components, deposits of native sulfur are formed, and the precipitation of base metal is thereby suppressed because of the high acidity of the generated hydrothermal solutions. The involvement of magmatic gases in an amount of a few percent in a hydrothermal system enhances the overall ore-generating potential of the system in terms of sulfide ores.

Keywords: hydrothermal vents, island arcs, thermodynamic simulations, massive volcanic sulfide ores, magmatic–hydrothermal systems

DOI: 10.1134/S0016702912130046

INTRODUCTION

The discovery of ore-forming hydrothermal systems at the seafloor was one of the greatest achievements in geology in the last quarter of the 20th century. Studies of submarine hydrothermal system are of importance for both fundamental academic science and applied geology. On the one hand, the possibility of immediate examination of hydrothermal ore-forming processes provides insight into hydrothermal processes as a

whole, and on the other hand, hydrothermal orebodies found on the seafloor were of prospective economic interest. Moreover, certain structural features of these systems provide invaluable information for the exploration for their ancient analogues onshore.

More than one hundred hydrothermal systems is so far discovered and variably thorough examined on the seafloor. Most of these systems were found on mid-oceanic ridges and spreading ridges in backarc basins.

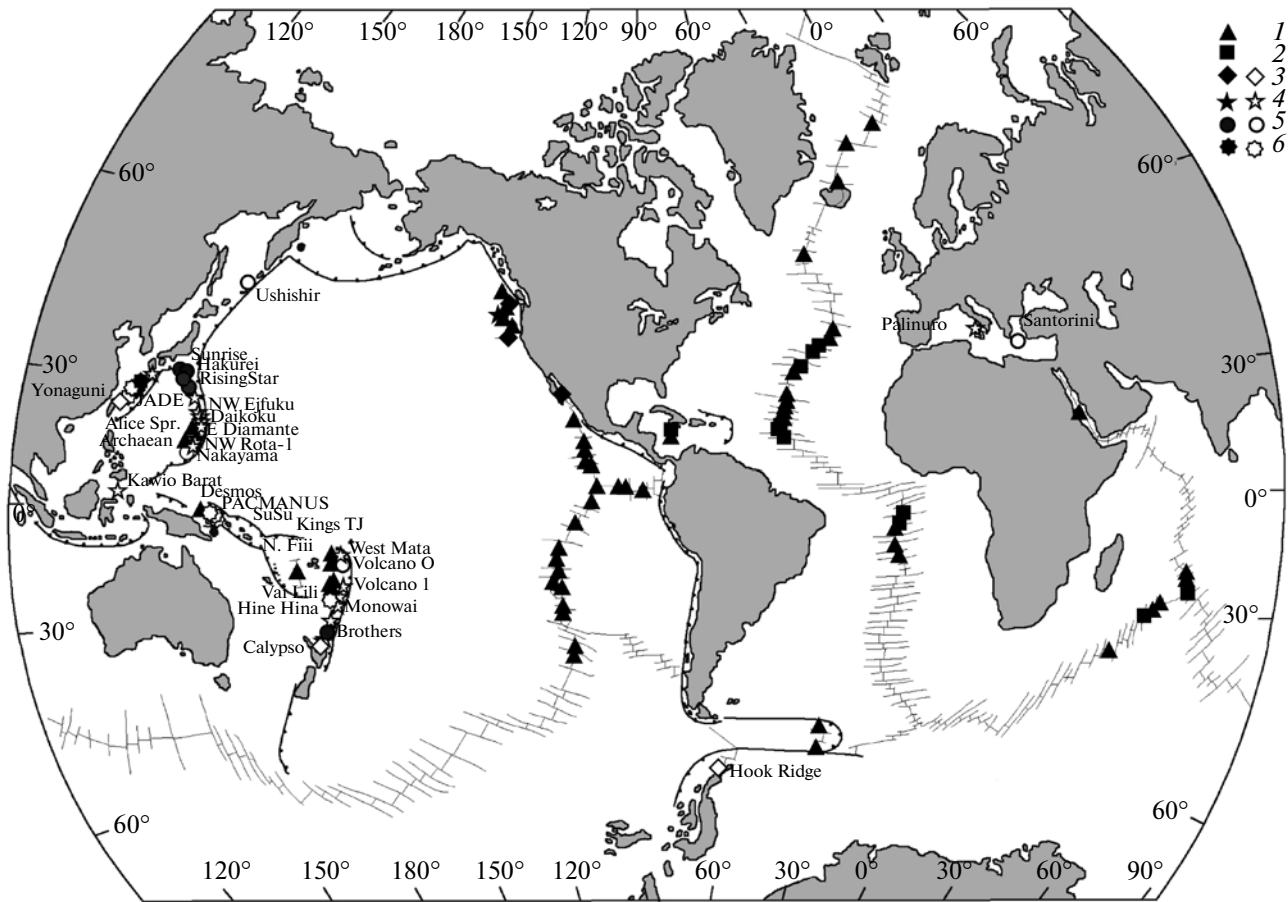


Fig. 1. Distribution of hydrothermal systems on the seafloor (based on data in [8]). Only geologically documented fields are shown.

1—Hydrothermal systems of spreading axes; 2—hydrothermal systems in massifs of ultramafic rocks; 3—littoral hydrothermal systems and hydrothermal systems in the sedimentary cover; 4—hydrothermal systems in the cones of active volcanoes; 5—hydrothermal systems in the calderas of submarine volcanoes; 6—hydrothermal systems in volcanic ridges. Solid symbols corresponds to hydrothermal systems producing massive sulfide ores, open symbols show hydrothermal systems precipitating native sulfur.

Over the past two decades, such active hydrothermal systems were also found in island arcs, mostly in the western Pacific Ocean (Fig. 1).

In comparing the importance of these discoveries, it should be taken into account that ancient sulfide deposits that are usually thought to be analogous to modern sulfide ores on the seafloor were likely produced not in the environments of mid-oceanic ridges but almost exclusively in arc environments. The resources of ancient ore deposits are a few orders of magnitude greater than those of most modern ore occurrences discovered in mid-oceanic ridges (MOR), and only occasional orebodies comprising a few million tons of ore are comparable with onshore ore deposits (TAG, Zenith-Victoria, Middle Valley, and others [6, 7]). A few ore accumulations found so far in the hydrothermal systems of island arcs have masses of the order of millions of tons: these are Sunrise in the Myojin Knoll caldera (about nine million

tons [8]) and Hakurei in the Bayonaise Knoll caldera in the Izu-Bonin arc [9, 10], Solwara 1 in the East Manus backarc basin (2.78 million tons [11]), and also likely Hatoma Knoll in the Okinawa arc [8]. Hopefully, modern submarine arc-related orebodies are, like their ancient analogues, greater than in MAR.

Hydrothermal systems in modern island arcs are examined incomparably less thoroughly than in mid-oceanic ridges [6], and when this paper was written, no more than 3% of the total length of island arcs was systematically studied. Systematic data available so far were obtained by Japanese geologists on the Okinawa and Izu-Bonin arcs in the Japanese economic zone (see the review in [8]). Extensive data were lately obtained by a number of American and American–New Zealand expeditions that worked at submarine volcanoes in the Mariana and Tonga-Kermadec island arcs and hydrothermal systems in the East Manus backarc basin [12–15, and others].

The results of these studies indicate that hydrothermal activity is widespread at active submarine volcanoes in island arcs (Fig. 1). For example, such activity of variable intensity was detected in the Tonga-Kermadec arc at 13 submarine volcanoes [16]. Hydrothermal fields in these geodynamic environments are typically spatially restricted to areas near the walls of the calderas of submarine volcanoes and to young volcanic cones. The fact that hydrothermal activity is localized in such areas was previously documented at mid-oceanic ridges, with hydrothermal systems occurring at seamounts (as at Axial Seamount in the Juan de Fuca Ridge and 13° N Seamount in EPR) and Loihi submarine volcano.

As was demonstrated in [12 and others], the tactics of searches for hydrothermal systems developed for mid-oceanic ridges proves not to be as efficient when applied in island arcs and should be fundamentally revised. The methods worked out by American and New Zealand researchers are based primarily on the identification of geochemical anomalies in the water and subsequent searches for the sources of these anomalies (hydrothermal systems). However, experience gained so far suggests that some of these systems bear no significant sulfide mineralization, and this calls for the development of additional criteria that would allow focusing searches to certain segments of island arcs.

This can be done based on understanding the mechanisms and conditions forming sulfide ore mineralization on the seafloor, including the geology of island arcs. Judging from currently available information, having generally closely similar geochemistry to that of thoroughly examined hydrothermal systems in mid-oceanic ridges, hydrothermal systems in island arcs and mid-oceanic ridges still exhibit certain differences from their analogues in mid-oceanic ridges. It is quite difficult to interpret the nature of these differences based solely on available observation results, and moreover, these interpretations are far from always unambiguous. Additional data for such interpretations can be provided by the thermodynamic simulations of processes that occur in the hydrothermal systems of island arcs.

Currently available materials indicate that the morphologies of orebodies and the mechanisms of the ore-forming processes in hydrothermal systems in these environments are generally similar. The ore mineralization is produced at a rapid temperature decrease when the hydrothermal solution ascending to the seafloor surface is mixed with cold bottom seawater. The assemblages of major ore minerals are also similar and comprise the most widely spread sulfides of ore metals, such as pyrite, chalcopyrite, sphalerite, and marcasite. At the same time, these assemblages persistently show certain differences in their associations of minor min-

erals and elements. For example, hydrothermal systems in island arcs are reportedly richer in Pb, As, and Sb, contain realgar and orpiment, which are atypical of ores in mid-oceanic ridges [8 and others].

Based on general geological considerations, it can be expected that differences between ore-forming processes in island arcs and mid-oceanic ridges can be accounted mostly by (1) differences in the composition of the crustal rocks (mafic–acid rocks instead of basalts and serpentinite and the occurrence of sedimentary material), (2) shallower depths of both the magmatic sources and the levels of ore deposition, and (3) the longer lifetimes of the heat sources.

*Geological and geochemical indications
of the involvement of magmatic fluids
in ore-forming processes in island arcs*

The problem of the involvement of magmatic fluid in processes forming sulfide ore mineralization has long been explored by several researchers [17 and others]. The contribution of magmatic fluids to ore-forming processes in modern hydrothermal systems in mid-oceanic ridges is insignificant (see reviews in [18, 19]), but several geologists are prone to believe that the contribution of magmatic fluids in island arcs is, conversely, very significant [20–22 and others].

This viewpoint was initially based on the discovery of high concentrations of ore-forming elements in inclusions in magmatic rocks and has lately received further support from finds of unusual (compared to those in mid-oceanic ridges) hydrothermal vents in backarc spreading centers and then in island arcs. Such hydrothermal systems were first discovered in the Manus (DESMOS submarine caldera [23]) and Lau (Hine Hina field [24]) basins. The fluid of these systems was extremely acidic (pH < 2), their hydrothermal deposits contained native sulfur and alunite, the gas concentrations were very high, and the sulfur isotopic composition of the sulfide and native sulfur was unusually light (in samples from the Hine Hina field, $\delta^{34}\text{S}$ was from -7.7 to -2.8% for pyrite and from -4.8 to -2.4% for native sulfur). All of these features were convincingly explained in the aforementioned publications as resulting from the influx of magmatic gases containing SO_2 . The disproportionation of SO_2 during its cooling and dissolution in seawater gives rise to sulfate solutions and native sulfur and is associated with sulfur isotopic fractionation.

Hydrothermal systems with the aforementioned features, first of all, with native sulfur, were later found elsewhere in the Manus backarc basin (North Su [25]), Mariana arc (NW Rota-1 [26], TOTO caldera [27], and others), Kermadec arc (cone of Brothers submarine volcano [12, 28]), and in the Bransfield Strait [29] (Fig. 1). Note that no significant sulfide

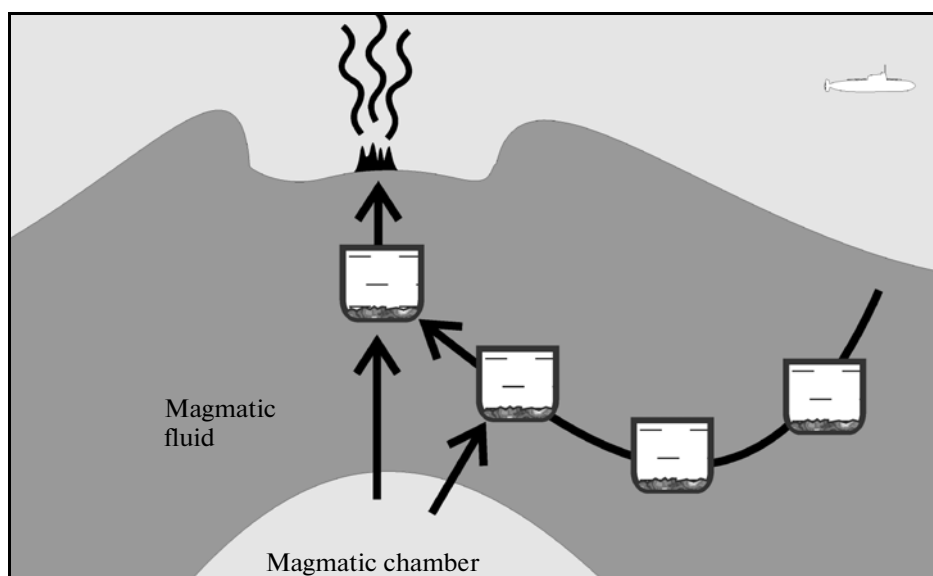


Fig. 2. Principal structural scheme of the model of a hydrothermal system in an island arc.

orebodies have ever been found in these hydrothermal systems.

Considered collectively, the facts and considerations presented above demonstrate that a magmatic fluid source must be taken into account in the geological–geochemical model of hydrothermal systems in island arcs.

Geological–geochemical model of a hydrothermal system in the island-arc crust

The geological prototype of such a system was assumed to be the caldera of a submarine volcano composed of rocks of various composition, with heat and fluids coming from a magmatic source (Fig. 2).

The general scheme of the process is as follows. Under the effect of a heat source (a magmatic chamber), seawater permeating fractured rocks in the caldera is involved in large-scale thermal convection. Being heated, the seawater starts to interact with the rocks and metasomatize them, the composition of the water is modified, and it is transformed into a ore-forming fluid. Near the magmatic chamber, the hydrothermal solution of marine origin is mixed with magmatic fluid (condensate of volcanic gases). The discharge of the hydrothermal solution at the seafloor is associated with a drastic temperature decrease and, consequently, the precipitation of ore material.

A technique for the thermodynamic simulation of such a scenario of the hydrothermal process was suggested in our earlier publications [1, 19]. This technique is based on the calculation of the state of a flow-through multistep reactor that imitates the evolution of geochemical processes along the convection flow

line of the hydrothermal solution. Variations in the simulation parameters (temperature, pressure, and the rock/water ratio) and the simulation of the passage of sequential solution portions through the multistep reactor allowed us to take into account the changing chemistry of the process and to reproduce its evolution with time. The model simulated in this publication differs from our earlier models in that it involves more diverse compositions of the rocks that interact with hydrothermal solution.

In contrast to oceanic crust that almost completely consists of tholeiites, the island arc crust is made up of diverse magmatic rocks, which range from mafic calc–alkaline basalts to acid rocks. In this model, the effect of this compositional diversity is taken into account via simulating the interaction of hydrothermal solutions with rocks of four discrete compositions: calc–alkaline basalt, andesite, dacite, and rhyolite. In order to make our simulation results comparable with our earlier models for the hydrothermal process in mid-oceanic ridges [1, 19], we have simultaneously simulated interactions with tholeiite (MORB).

The starting major-component compositions of the rocks were compiled from [30] and were regarded as typical rocks in the transitional (island arc) crust. The trace-element compositions of the rocks was approximated by the respective abundances of trace elements in the rocks in [31]. The rock compositions used herein are listed in Table 1.

In studying hydrothermal systems in island arcs, it is particularly interesting to explore the possibility of the involvement of sedimentary rocks (which are atypical of mid-oceanic ridges) in the generation and evolution of the hydrothermal solutions. To estimate this

Table 1. Average rock compositions utilized in the model (after [30, 31])

| Component | Concentration unit | Calc-alkaline basalt | Andesite | Dacite | Rhyolite | Calcareous terrigenous sedimentary rock |
|--------------------------------|--------------------|----------------------|----------|--------|----------|---|
| SiO ₂ | wt % | 50.76 | 60.22 | 66.9 | 75.7 | 39.72 |
| TiO ₂ | same | 1.11 | 0.63 | 0.55 | 0.27 | 0.563 |
| Al ₂ O ₃ | same | 17.62 | 17.09 | 17.25 | 13.16 | 9.51 |
| Fe ₂ O ₃ | same | 3.64 | 3.82 | 1.73 | 0.66 | 3.34 |
| FeO | same | 5.88 | 3.65 | 2.02 | 0.72 | 1.31 |
| MnO | same | 0.18 | 0.08 | 0.11 | 0.08 | 0.26 |
| MgO | same | 6.58 | 3.9 | 1.36 | 0.42 | 2.13 |
| CaO | same | 10.17 | 5.19 | 3.17 | 0.96 | 19.18 |
| Na ₂ O | same | 2.87 | 3.8 | 4.07 | 3.61 | 1.43 |
| K ₂ O | same | 0.89 | 1.42 | 2.63 | 4.34 | 1.51 |
| P ₂ O ₅ | same | 0.3 | 0.2 | 0.21 | 0.09 | 0.198 |
| C _{org} | same | — | — | — | — | 0.11 |
| CO ₂ | same | — | — | — | — | 14.29 |
| SO ₃ | same | — | — | — | — | 0.355 |
| Cl | same | — | — | — | — | 0.136 |
| H ₂ O | same | — | — | — | — | 5.94 |
| S | ppm | 250 | 200 | 250 | 300 | 380 |
| Cu | same | 100 | 55 | 40 | 20 | 60 |
| Zn | same | 110 | 72 | 66 | 60 | 90 |
| Pb | same | 8 | 10 | 15 | 20 | 20 |
| As | same | 2 | 2 | 2 | 1.5 | 6.6 |
| Sb | same | 0.2 | 0.2 | 0.2 | 0.2 | 0.2 |
| Ag | same | 0.1 | 0.1 | 0.08 | 0.05 | 0.1 |
| Au | same | 0.004 | 0.003 | 0.0035 | 0.004 | 0.001 |

factors, we have conducted simulations in which the crustal rock sequences included sedimentary rocks. The composition of the sedimentary rocks was assumed to be an average of the data reported in [30] for the transitional crust. These rock sequences differ from purely magmatic ones in containing carbonates, organic carbon, hydrated minerals, and sulfate sulfur (Table 1).

Evaluated composition of magmatic gas

Inasmuch as the composition of the magmatic gas is one of the most important parameters of our model, we have preliminarily evaluated the variations in the composition of magmatic fluids in an island arc environment. Using a compilation of data on the composition of gases and volcanic condensates sampled worldwide, we composed a database of representative trace-element compositions of volcanic gases from 25 active volcanoes, including fourteen volcanoes at island arcs: Alaid, Ebeko, Kudryavy, Showa Shinzan, Usu, Satsuma-Iwo Jima, Tangkuban Parahu, Papan-

dayan, Merapi, Vulcano, and others. For all samples included in database, high (>400°C) temperatures of the gases at the moment of their sampling ensure that these gases were not any significantly contaminated by atmospheric air. The trace-element composition of the volcanic fluids was determined by recalculating the composition of the condensates of volcanic gases. Currently reliable (judging from the sampling and analytical techniques) data on a broad spectrum of trace element are available for eight active volcanoes, including five in island arcs (Alaid, Ebeko, Kudryavy, Merapi, and Momotombo) and three on active continental margins (Augustine, St. Helens, and Tolbachik). All of the condensates were sampled at fumaroles whose temperatures exceeded 450°C. The analyses are summarized in Table 2.

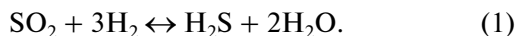
The analysis of the integrated information shows that the most reliable and exhaustive information is that on Kudryavy andesite stratovolcano on Iturup Island. Gases from this volcano were independently analyzed by several research teams, and their results were consistent [3, 32–35]. The concentrations of

Table 2. Concentrations (ppm) of elements in the condensates of volcanic gases

| Element | Temperature, °C | | | | | | | | | | Black smoker at 21°N EPR [44] | | |
|-----------|---------------------|-------|---------------------|--------------------|-------------------|---------------|---------------|----------------|--------------------|------|----------------------------------|-----------|-------|
| | Kudryavy [3, 32–35] | | August- ine [36] | St. Helens [37] | Tolbachik [38] | Alaid [39] | Ebeko [40] | Merapi [41] | Momotombo [42, 43] | | | | |
| | 585 | 825 | 870 | 940 | 870 | 710 | 930–1020 | >700 | – | 790 | 456–770 | 880 | 351 |
| 1 | 2 | 3 | 4 | 5 | 6 | 7 | 8 | 9 | 10 | 11 | 13 | 14 | 15 |
| Na | 22.5 | 5 | 41.2 | 6.1 | – | 5.2 | 281 | – | 15.4 | – | – | – | 10200 |
| K | 12.8 | 9.53 | 28.6 | 5.62 | – | 3.9 | 302 | – | 4.7 | – | – | – | 934 |
| Mg | 1.7 | 0.88 | 1.76 | 0.5 | – | 0 | 8.1 | – | – | – | – | – | 0 |
| Ca | 5 | 1.73 | 5.5 | 2 | – | 0.010 | 11 | – | – | – | – | – | 469 |
| Al | 9.65 | 7.1 | 13 | 3.9 | – | 2.4 | 84 | – | – | – | – | – | 0.121 |
| Si | 184 | 98.8 | 197 | 79.1 | – | – | – | – | – | – | – | – | 438 |
| S | – | 123 | – | 215 | – | – | – | – | – | 257 | – | – | 269 |
| Cl (g/kg) | 12.21 | 12.85 | 15.38 | 8.58 | – | – | – | – | 4.053 | 3.5 | – | – | 17.58 |
| Mn | 0.12 | 0.055 | 0.21 | 0.09 | – | 0.0030 | 0.36 | – | – | 0.18 | – | 0.1–1.2 | 48 |
| Fe | 3.7 | 3.62 | 6.8 | 7.3 | 4.0 | 0.20 | 32 | 48.2 | 16.4 | 9 | 8.1–50 | 1–36 | 136 |
| Co | <001 | 0.003 | 0.016 | 0.006 | – | 0.00039 | 0.018 | – | – | – | – | – | 0.013 |
| Ni | 0.05 | 0.32 | 0.055 | 0.41 | – | 0 | 0.36 | – | – | – | – | – | – |
| Cu | 0.032 | 0.09 | 0.13 | 0.27 | 0.20 | 0.053 | 6.4 | 0.48 | 0.74 | 0.09 | 0.2–8 | 0.1–1.5 | 2.8 |
| Zn | 0.58 | 1 | 1 | 3.1 | 1.9 | 0.020 | 33 | 25.2 | 11.6 | 10 | 0.4–76 | 0.4–6 | 6.8 |
| As | 0.73 | 1.25 | 1.55 | 1.2 | 3.3 | 1.4 | 8.3 | – | – | 0.53 | 0.2–0.5 | 2–5.5 | 0.034 |
| Ag | – | 0.096 | – | 0.135 | – | 0.00002 | 0.003 | – | – | – | 0.015 | 0.005 | 0.004 |
| Cd | 0.23 | 0.88 | 0.58 | 0.23 | 0.11 | 0.04 | 1.07 | 1.44 | 0.219 | 0.2 | 0.02–0.7 | 0.01–0.18 | 0.02 |
| Sb | 0.24 | 0.1 | 0.02 | 0.079 | 0.21 | 0.008 | 16 | 0.38 | 0.57 | <0.6 | 0.003–0.1 | 1.7 | – |
| Hg | 0.075 | 0.025 | 0.015 | 0.028 | – | 0.02 | 0.063 | – | – | – | – | – | – |
| Pb | 1.84 | 0.11 | 0.08 | 1.25 | 2.2 | 0.54 | 1.42 | 0.72 | 0.58 | 0.8 | 2–7 | 0.05–0.6 | 0.074 |

most components in gases and condensates from Kudryavyi volcano are close to the median values of the whole databank.

We have demonstrated [1] that the simulation results on ore-forming processes in a hydrothermal system fed by magmatic fluid significantly depend on the pressure under which magmatic gas is separated from the melt. As was established in [45], the proportions of oxidized and reduced sulfur species in gas in equilibrium with magma are controlled by the reaction



As follows from the equation for the equilibrium constant of reaction (1),

$$X_{\text{H}_2\text{S}}/X_{\text{SO}_2} = K_1 P_{\text{tot}} \left(X_{\text{H}_2}^3 / X_{\text{H}_2\text{O}}^2 \right), \quad (2)$$

where X_i is the mole fraction of component i in the gas phase. The proportions of sulfur species thus depend on the redox conditions and total pressure in the system. The equilibrium is shifted toward H_2S at a high pressure and low oxygen fugacity and toward SO_2 and a low pressure and high oxygen fugacity. The redox properties of a magmatic system at its degassing are controlled by the composition of the melt, first of all, by the ratio of species with Fe of different valence.

In order to estimate the role of this phenomenon, we have invented [1] a procedure for introducing a pressure correction into the composition of magmatic gas at a degassing pressure. The procedure involved the solution of an auxiliary problem of thermodynamic equilibrium of magmatic gas with the *QFM* (quartz–fayalite–magnetite) buffer at a temperature of 1000°C and variable pressure. The calculations were conducted using the HCh program package and the assumption of an ideal mixture of ideal gases. The calculated equilibrium gas composition was then utilized as a starting point for simulating the hydrothermal ore-forming process. The results thus obtained demonstrate that the boundary line between the H_2S - and SO_2 -dominated ranges runs between 50 and 100 bars, which corresponds to a seawater depth of 500–1000 m at a hydrostatic pressure or a rock thickness of 200–400 m at a lithostatic pressure.

Comparison with observation results on hydrothermal systems in island arcs suggests that indications that SO_2 is introduced into hydrothermal systems (for example, the occurrence of native sulfur in the sediments) were discerned at depths greater than in the model: 1.5–2.0 km. This implies that the aforementioned results are provisional, and the model of melt degassing should be further adjusted.

The following two specifying issues were then introduced into the model:

1. We have modified the technique for the calculation of the properties of the gas phase. In the preparatory calculations, the magmatic gas was treated in an

ideal approximation (as an ideal mixture of ideal gases). The HCh version 4.x program package provides the possibility of more accurate treating the magmatic gas, namely, as a real gas whose properties are described by the modified PRSV2 (Peng–Robinson) model [46, 47].

2. We have taken into account the fact that the redox characteristics of arc magmatic melts differ from *QFM* (are more strongly oxidized) and approach the Ni–NiO buffer [48]. In the final variant, the simulations were made for conditions of oxygen fugacity f_{O_2} exceeding that in equilibrium with the *QFM* buffer by one unit (*QFM* + 1).

The results of these more accurate simulations are exhibited in Fig. 3. It can be seen that the region dominated by SO_2 is expanded to a pressure of 200 bars, and minor SO_2 amounts can be present at even higher pressures. This correction eliminates the inconsistency between the preparatory calculations and natural observations.

In simulating hydrothermal processes, we assumed the calculated compositions of magmatic gas at pressures of 100 and 500 bars, which corresponds to a “shallow-sitting” (at a depth of less than 1 km) magmatic chamber and a “deep-sitting” (water depth of 2 km plus more than 1 km of rocks above the roof of the magmatic chamber beneath the caldera).

Thermodynamic model

The simulations were carried out for a 19-element chemical system H–O–K–Na–Ca–Mg–Fe–Al–Si–C–S–Cl–Cu–Zn–Pb–As–Sb–Ag–Au at temperatures of 25–370°C and pressures of 10–500 bars. The simulated multisystems involved 88 possible minerals, aqueous solution with 95 simple and complex ions and molecules, and gas solution consisting of eight components. The list of the minerals, aqueous and gaseous species in the corrected model is presented in Tables 3 and 4.

Thermodynamic properties of various compounds were calculated using the UNITHERM databank and were generally consistent with those utilized in [1, 19]. The database version used in our research was corrected based on the results of recent generalizations and experimental studies.

1. The properties of Cu, Ag, and Au simple ions and complexes (except only for Cu chloride complexes) were taken according to [49].

2. The properties of Cu chloride complexes were assumed according to [50].

3. The properties of arsenopyrite and $\text{H}_3\text{AsO}_3^\circ$ were assumed according to [51].

4. The properties of stibnite and $\text{Sb}(\text{OH})_3^\circ$ were compiled from [52].

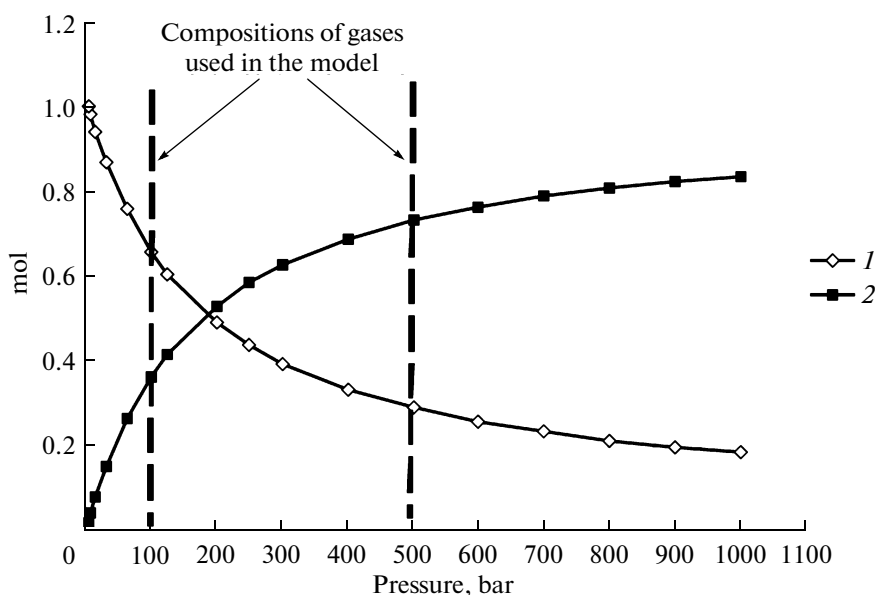


Fig. 3. Thermodynamic calculation of the proportions of sulfur species in magmatic fluid as a function of pressure. Simulation parameters: $T = 1000^{\circ}\text{C}$, *QFM + 1 buffer*, the bulk composition of the gas corresponds to that of gas from Kudryavy volcano. 1— SO_2 ; 2— H_2S .

5. The properties of gas solutions were approximated by the modified Peng–Robinson PRSV2 model [46, 47] with regard for the properties of real gases and nonideality of mixing.

The quality of the utilized data was tested by comparing with an independent summary of properties of compounds [53]. This comparison indicates that discrepancies between respective data in UNITHERM and in [53] are within the errors of the initial experimental data, which testifies that the quality of the input thermodynamic information for our simulations is high enough.

The simulation of the migration of minor chalcophile elements (Sb and Ag in our model) is notably complicated by the fact that the predominant mode of their precipitation in nature is their incorporation as isomorphous components in crystallizing sulfides. If no individual minerals of these elements are assumed in the simulations to be formed in the equilibrium mineral assemblage, the migration capability of these elements can be significantly overestimated, and this can lead to geochemical misinterpretations. A way out of this situation was found by introducing two solid solution minerals: sphalerite as a $\text{ZnS}-\text{Ag}_2\text{S}$ solid solution and fahlore as a multisite Fe–Zn solid solution (of tennantite–tetrahedrite end members). This allowed us to more reliably simulate the behavior of Ag and Sb as minor elements. Note that the assumption of the geochemically more common occurrence of Ag as an isomorphous component of galena fails to lead to the desired goal because of the small stability field of galena in the hydrothermal system.

The simulations were carried out with the HCh program package [54, 2] in compliance with the technique earlier suggested in [1, 19]. The general parameters of the model were as follows: the temperature of the descending branch was increased from 150 to 370°C at a step of 10°C (23 steps), and the pressure was constant: 500 bars. The introduction of fresh rock into the interactions was increased exponentially, from 1 g per 1 kg of solution at the first step to 1 kg (total) per 1 kg of solution in the descending branch. The generated solution was brought to the first step, whose temperature was 150°C and the pressure was 200 bars (the ore deposition conditions were assumed according to what is typical of known hydrothermal systems in island arcs).

Simulation of the inner structure of a growing orebody

The simulation of the inner structure of a growing orebody fed by hydrothermal solutions coming from a system that evolves with time is an independent challenge and a fairly complicated problem.

This problem can also be resolved using the MFTMR technique but requires a much more complicated procedure for specifying the composition of the discrete steps of the flow-through reactor [4]. In [4], this was implemented in the specialized GRDEP computer program, which involved the solution of a thermal problem and the simulation of equilibria at discrete steps using a simplified version of the Gibbs computer program. The ability of the newly developed version of the HCh program package to address the

Table 3. List of minerals involved in the thermodynamic model for an island arc hydrothermal system

| | | | |
|--------------|--------------|----------------|-----------------|
| Hematite | Siderite | Clinocllore | Realgar |
| Magnetite | Cerussite | Chlorite25* | Orpiment |
| Chalcocite | Smithsonite | Chlorite50* | Arsenopyrite |
| Chalcopyrite | Anglesite | Chlorite75* | Stibnite |
| Bornite | Diaspore | Daphnite | Fe-freibergite |
| Galena | Kaolinite | Tremolite | Zn-freibergite |
| Troilite | Pyrophyllite | Actinolite20* | Cu-tennantite |
| Pyrite | Sillimanite | Actinolite40* | Cu-tetrahedrite |
| Anhydrite | Albite | Actinolite60* | Skinnerite |
| Gypsum | Microcline | Actinolite80* | Chalcostibite |
| Alunite | Anorthite | Ferrotremolite | Miargyrite |
| Sulfur | Wairakite | Zoisite | Pyrargyrite |
| Copper | Forsterite | Epidote33* | Proustite |
| Silver | Fayalite | Epidote67* | Bulangerite |
| Gold | Enstatite | Pistacite | Bournonite |
| Graphite | Ferrosilite | Paragonite | Pearceite |
| Quartz | Diopside | Sericite50* | Polybasite |
| Brucite | Wollastonite | Muscovite | Zinkenite |
| Goethite | Talc | Heulandite | Enargite |
| Calcite | Chrysotile | Halite | Berthierite |
| Magnesite | Prehnite | Chlorargyrite | Sphalerite** |
| Dolomite | Pumpellyite | Covellite | Fahlore*** |

Notes: * Intermediate compositions of the solid solutions of rock-forming minerals: the numerals indicate the mole fractions of Fe end members for chlorite, actinolite, and epidote and the K end member of sericite;

** Sphalerite as a solid solution of ZnS and Ag₂S;

*** Fahlore as a multisite a solid solution of Fe–Zn tennantite and tetrahedrite.

Gibbs program from the user's programs with the application of the OLE Automation technology (a technology of "openness from above" [2]), makes it possible to generate as complicated as desired mass transfer models in applications compatible with the OLE technology, for example, MS Excel.

Ore precipitation on the seafloor initially proceeds due to mixing of hydrothermal solution with bottom seawater because of the drastic decrease in the solution temperature and changes in its chemical composition. Upon the origin of an "embryo" orebody, which is partly cooled via conductive heat loss, ore material precipitates both inside the growing orebody (because of the temperature gradient) and on its surface (because of the discharge of the hydrothermal solution).

Theoretical aspects of the simulation of the development of a hydrothermal-precipitate orebody are discussed in much detail in [4, 19]. A model for the ore precipitation zone should include two constituents: one of them describes the processes of material precipitation and replacement during solution filtration within the orebody, and the other one deals with the precipitation of material on the surface of the body,

when the discharged solution mixes with ambient seawater (Fig. 4). The reactor emulating the ore deposition zone differs from others in that the boundaries of the temperature steps are displaced with time because of the growth of the orebody. As a result, the material deposited at a certain temperature is eventually displaced into a region of higher temperature, which is one of the principal reason for the metasomatic replacements of the previously deposited ore material and the development of zoning in the orebody. To construct a thermodynamic model for a growing orebody, one should know the temperature in this body and on its surface and the growth rate of the body. The temperature distribution within the orebody controls the zoning of ore material precipitation, and the temperature on the surface of the body predetermines the fraction and composition of the material precipitated during mixing with seawater. The growth of the body should cause variations in these parameters with time.

Thermal model for an ore edifice. The orebody in the thermal model can be approximated by a hemisphere of radius R and with a center at the point from which the ore-forming solution comes (Fig. 5). The

Table 4. List of solute and gaseous compounds involved in the thermodynamic model for an island-arc hydrothermal system

| Components of aqueous solution | | | | |
|--|----------------------------------|---------------------------------|----------------------------------|---|
| H ₂ O | Na ⁺ | Ca ⁺² | Zn ⁺² | Fe ⁺² |
| H ⁺ | NaOH ^o | CaOH ⁺ | ZnOH ⁺ | FeOH ⁺ |
| OH ⁻ | NaCO ₃ ⁻ | CaCO ₃ ^o | ZnHCO ₃ ⁺ | Fe(OH) ₂ ^o |
| H ₂ ^o | NaHCO ₃ ^o | CaHCO ₃ ⁺ | ZnCl ⁺ | Fe(OH) ₃ ⁻ |
| O ₂ ^o | NaSO ₄ ⁻ | CaSO ₄ ^o | ZnCl ₂ ^o | FeSO ₄ ^o |
| H ₄ SiO ₄ ^o | NaCl ^o | CaCl ⁺ | ZnCl ₃ ⁻ | FeCl ⁺ |
| H ₂ S ^o | K ⁺ | CaCl ₂ ^o | ZnCl ₄ ⁻² | FeCl ₂ ^o |
| HS ⁻ | KCl ^o | Cu ⁺ | Ag ⁺ | FeOHCl ^o |
| SO ₄ ⁻² | Mg ⁺² | CuOH ^o | AgCl ^o | FeOHC1 ₂ ⁻ |
| HSO ₄ ⁻ | MgOH ⁺ | CuCl ^o | AgCl ₂ ⁻ | Fe(OH) ₂ Cl ⁻ |
| HAsO ₃ ⁻² | MgCO ₃ ^o | CuCl ₂ ⁻ | AgCl ₃ ⁻² | Fe(OH) ₂ ⁺ |
| H ₂ AsO ₃ ⁻ | MgHCO ₃ ⁺ | CuCl ₃ ⁻² | Ag(HS) ₂ ⁻ | Fe(OH) ₃ ^o |
| H ₃ AsO ₃ ^o | MgSO ₄ ^o | CuCl ₄ ⁻³ | Au ⁺ | Fe(OH) ₄ ⁻ |
| HAs ₂ S ₄ ⁻ | MgCl ⁺ | Pb ⁺² | AuOH ^o | Fe(OH) ₂ Cl ^o |
| Sb(OH) ₃ ^o | MgCl ₂ ^o | PbOH ⁺ | AuHS ^o | Fe(OH) ₃ Cl ⁻ |
| Sb(OH) ₂ ⁺ | MgOHCl ^o | PbCl ⁺ | Au(HS) ₂ ⁻ | CO ₃ ⁻² |
| Sb(OH) ₄ ⁻ | Al(OH) ₂ ⁺ | PbCl ₂ ^o | AuCl ₂ ⁻ | HCO ₃ ⁻ |
| H ₂ Sb ₂ S ₄ ^o | Al(OH) ₃ ^o | PbCl ₃ ⁻ | Cl ⁻ | H ₂ CO ₃ ^o |
| HSb ₂ S ₄ ⁻ | Al(OH) ₄ ⁻ | PbCl ₄ ⁻² | HCl ^o | CH ₄ |
| Components of gaseous solution | | | | |
| H ₂ O | H ₂ S | H ₂ | CH ₄ | HCl |
| CO ₂ | SO ₂ | O ₂ | | |

ore-forming solution filters through the orebody toward its surface (the tangential component of the filtration velocity is zero) and is then discharged into the bottom seawater. Heat is transferred within the orebody via two mechanisms: convective (with the solution) and conductive (due to the thermal conductivity of the solid material). Heat is lost to the ambient environment via the discharge of solution that passes through the orebody and via heat emission from the surface of the orebody. It is reasonable to assume that the thermal regime of the orebody is stationary because the body grows much more slowly than the heat is lost.

For the sake of simplicity, it was assumed that the thermal conductivity of the material composing the orebody and its filtration characteristics do not vary over the volume of the body. The heat capacity C and the density of the solution are assumed not to vary with temperature, and hence, the density component of solution convection within the orebody was ignored, as also was the heat loss through the bottom surface of the orebody. The condition of the spherical symmetry of the orebody allowed us to obtain an analytical solution of this problem (this solution was obtained by A.V. Tutubalin).

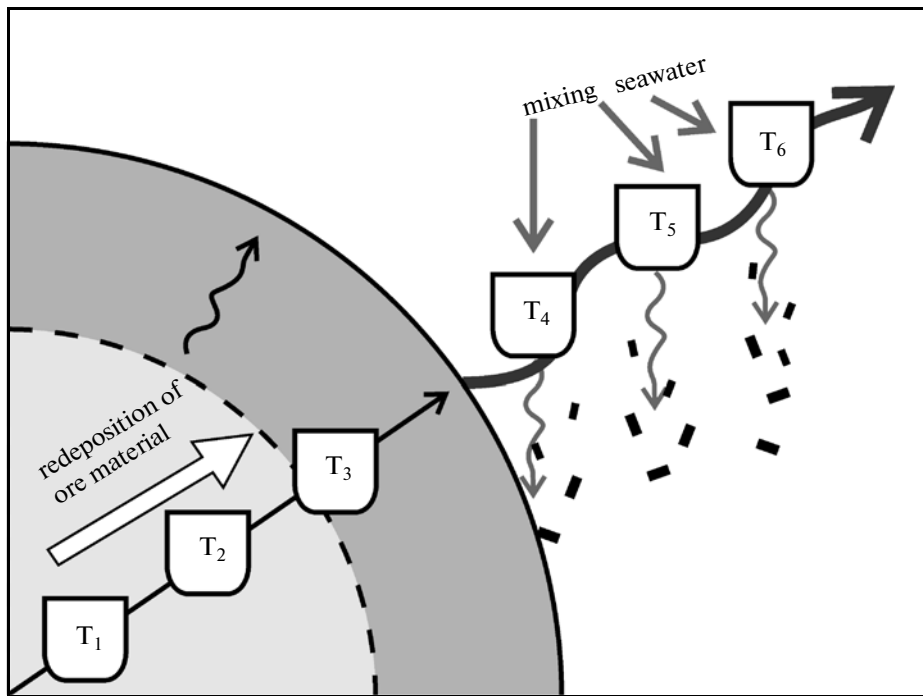


Fig. 4. Simulation scheme of a growing orebody.

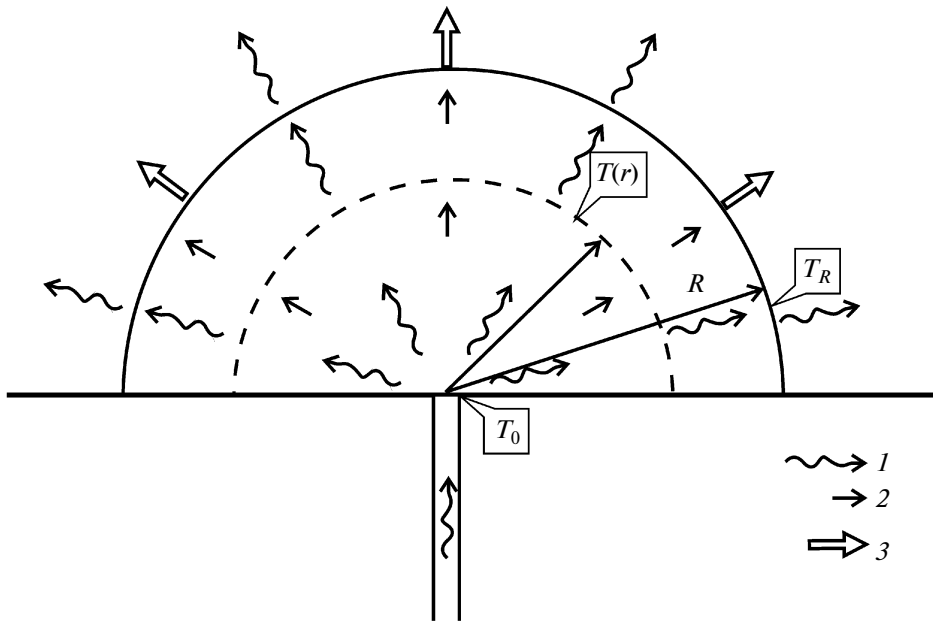


Fig. 5. Thermal model for the formation of an orebody. 1—Solution flow and convective heat transfer, 2—heat transfer via thermal conductivity, 3—heat loss from the surface.

The heat loss from the orebody surface to the environment can be described in our model by the Newton equation

$$\left(\frac{\partial Q}{\partial t}\right)_{cond}^- = \alpha S(T_R - T_{ext}), \quad (3)$$

where α is the heat loss coefficient, S is the surface area of the body (the surface area of a hemisphere of radius R is $S = 2\pi R^2$), T_R is the temperature at the surface, and T_{ext} is the temperature of the ambient bottom water (assumed to be 0°C).

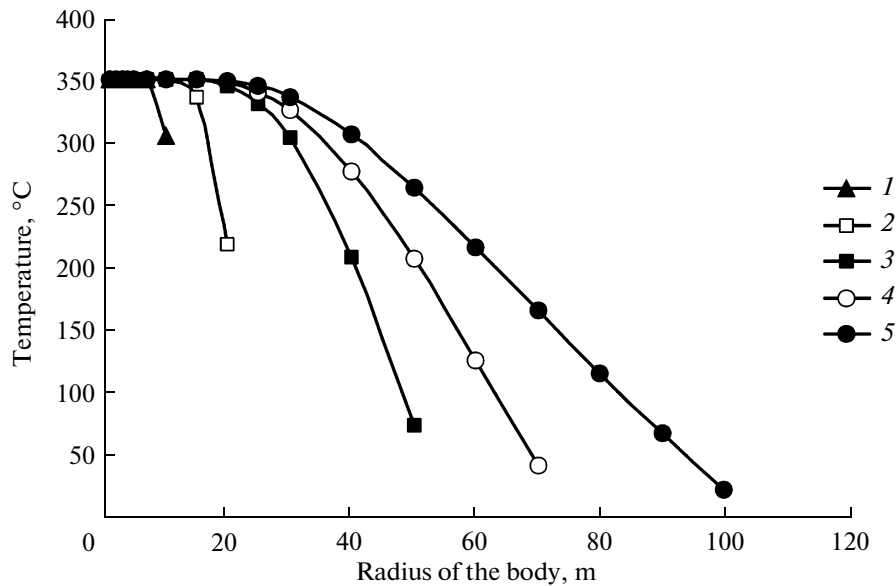


Fig. 6. Temperature distribution in a simulated orebody depending on its radius. The flow rate of the system is 100 kg/s. Radius of the body: 1—10 m; 2—20 m; 3—50 m; 4—70 m; 5—100 m.

The heat influx from the source is

$$\left(\frac{\partial Q}{\partial t}\right)^+ = qCT_o, \quad (4)$$

where q is the flow rate of the hydrothermal system, and T_o is the temperature of the source. The material balance condition for the solution coming from the source and discharged outside implies that the convective heat loss to the external environment is

$$\left(\frac{\partial Q}{\partial t}\right)_{conv}^- = qCT_R. \quad (5)$$

A stationary thermal state of the orebody requires a heat balance, which can be written using Eqs. (3)–(5) as

$$qCT_o = 2\pi R^2\alpha T_R + qCT_R. \quad (6)$$

This equation can be utilized to determine the temperature at the orebody surface

$$T_R = T_o \frac{qC}{2\pi R^2\alpha + qC}. \quad (7)$$

Heat transfer through an arbitrarily chosen spherical surface of radius r within the body consists of the convective heat transfer with solution and conductive heat transfer due to thermal conductivity, and the latter can be written as

$$\left(\frac{\partial Q}{\partial t}\right)_{r\,cond} = -\lambda S_r \frac{\partial T}{\partial r}, \quad (8)$$

where λ is the heat conductivity of the solid material. The heat transfer through any spherical surface should be the same due to the stationarity condition and

should be equal to the heat loss from the source, and hence, as follows from Eqs. (4), (5), and (8),

$$-2\pi r^2\lambda \frac{\partial T}{\partial r} + qCT(r) = qCT_o. \quad (9)$$

The solution of this equation is

$$T(r) = T_o + \gamma \exp\left(-\frac{qC}{2\pi\lambda r}\right), \quad (10)$$

where γ is the integration constant. This constant can be found by assuming $r = R$ and the value of $T(r)$ in Eq. (10) to be equal to $T(R)$ known from Eq. (7)

$$\gamma = -T_o \frac{2\pi\alpha R^2}{2\pi\alpha R^2 + qC} \exp\left(\frac{qC}{2\pi\lambda R}\right). \quad (11)$$

Substituting this expression into (1) and simplifying, we arrive at

$$T(r) = T_o \left\{ 1 - \frac{2\pi\alpha R^2}{2\pi\alpha R^2 + qC} \exp\left[\frac{qC}{2\pi\lambda} \left(\frac{1}{R} - \frac{1}{r}\right)\right] \right\}. \quad (12)$$

Figure 6 shows the temperature distribution calculated by Eq. (12) for bodies of various size at a constant flow rate of 100 kg/s from the source; this value was used in our later simulations by the model.

The progressive growth of the orebody can be described by the equation

$$M_n = \sum_{i=1}^n (\Delta S_i q \tau), \quad (13)$$

where M_n is the mass of the orebody after the passage of portion n of the solution from the descending branch of the system, ΔS_i is the mass of the ore mate-

rial precipitated from 1 kg of the hydrothermal solution in wave i (it is calculated in the thermodynamic model for the ore deposition zone and depends on the characteristics of the descending branch of the system), and τ is the discharge time of one solution portion. As follows from the results of earlier studies, the value of τ should be close to 10^8 s, i.e., approximately three years [19]. The following estimated values of the parameters were assumed in the pilot model: q is 100 kg/s, λ is 20 J/s cm² (which corresponds to a mixture of 75% silicates and 25% sulfides), α is 100 J/s cm² °C, and the heat capacity of water is 4184 J/g °C and is assumed not to vary with temperature.

The thermal model for the orebody allows us to specify the parameters of the flow-through reactor that approximates the submarine ore-forming process. This reactor consists of two “tandem” parts with different mass transfer mechanisms; the boundary between them is controlled by the surface temperature of the orebody, which can be calculated by Eq. (7). The first part pertains to the “interiors” of the orebody, in which material is precipitated because of a temperature decrease and the replacement of ore material precipitated earlier. The second part describes the mixing of the solution discharged from the edifice with ambient seawater. Inasmuch as it is convenient to carry out the thermodynamic simulations with discrete steps of the flow-through reactor having a constant temperature, the progressive growth of the orebody and the corresponding decrease in the temperature of its surface is associated with an increase in the number of steps pertaining to the interiors of the orebody and a respective decrease in the number of steps pertaining to the mixing zone. As the orebody grows via the deposition of fresh portions of ore material on its surface, the temperature steps gradually increase in volume and are shifted away from the mouth of the feeder. Because of this, the material precipitated earlier occurs in zones of progressively higher temperature, and the composition of the material at discrete temperature steps should be thus recalculated at each time step with regard for this factor. Under the effect of the solution, ore material within the body can be partly replaced and redeposited somewhere neared to the surface. The conditions of the second part of the reactor are specified by the heat balance of hydrothermal solution discharged at the surface of the body during mixing with bottom seawater. The whole mass of the thereby generated precipitate is added to the orebody during the next time step.

The mass of the orebody is thus increased upon the passage of each portion of the hydrothermal solution through the flow-through reactor in accordance with Eq. (13), and the volume is increased according to the increase in the total mass, the percentages of the deposited minerals, and their densities (the porosity of

the material is thereby neglected). This allowed us to calculate the current radius of the orebody for the next step, the temperature on its surface (by Eq. (7)), the number of temperature steps within and outside the body, and the radii of temperature steps within the body and the volumes of these steps, as well as to recalculate their new chemical compositions for interaction with hydrothermal solution.

An additional factor of the evolution of the orebody is the metasomatic transformation of the feeding part of the system, as was demonstrated in [19].

All of these characteristics and parameters of the heat transfer model were used in writing a specialized MS Excel macros. Starting to run after the calculation of a current state of the flow-through reactor at each step of the reactor and each time step, the macros addressed the HCh package to calculate the thermodynamic equilibria. Each of the calculated problems involved a flow-through reactor with 60 temperature steps, and up to 200 time steps (solution portions) were calculated, i.e., up to 12000 individual equilibrium calculations were carried out.

The calculations by the model provided equilibrium compositions of the solid phases and solutions (in the form of MS Excel spreadsheets) for temperature steps of the flow-through reactor (the descending and ascending branches and the ore deposition zone) for each calculation step, as well as the masses and radii of the temperature zones within the orebody. Since the physical structure of the orebody is determined by geometric parameters and data on temperature zones are illustrative, they were recalculated with regard for the different size of the temperature zones. Figure 7 shows an example of the calculation of the mineral composition of the model orebody produced by the activity of a hydrothermal system in andesitic crust at the 100th calculation step.

Simulation results

Our simulation results demonstrate that the generation of hydrothermal solution during seawater convection through heated island-arc rocks is generally similar to processes in hydrothermal systems in mid-oceanic ridges. The differences in the processes during the generation of hydrothermal solutions are quantitative. At the same time, the superposition of all of these differences can result in certain qualitative changes when the deposition of ore material and, particularly, its evolution with time are analyzed.

Effect of the composition of the igneous rocks. We simulated variants of the model that differed only in the composition of the rocks with which heated seawater interacted. This allowed us to identify the variability caused by this factor alone.

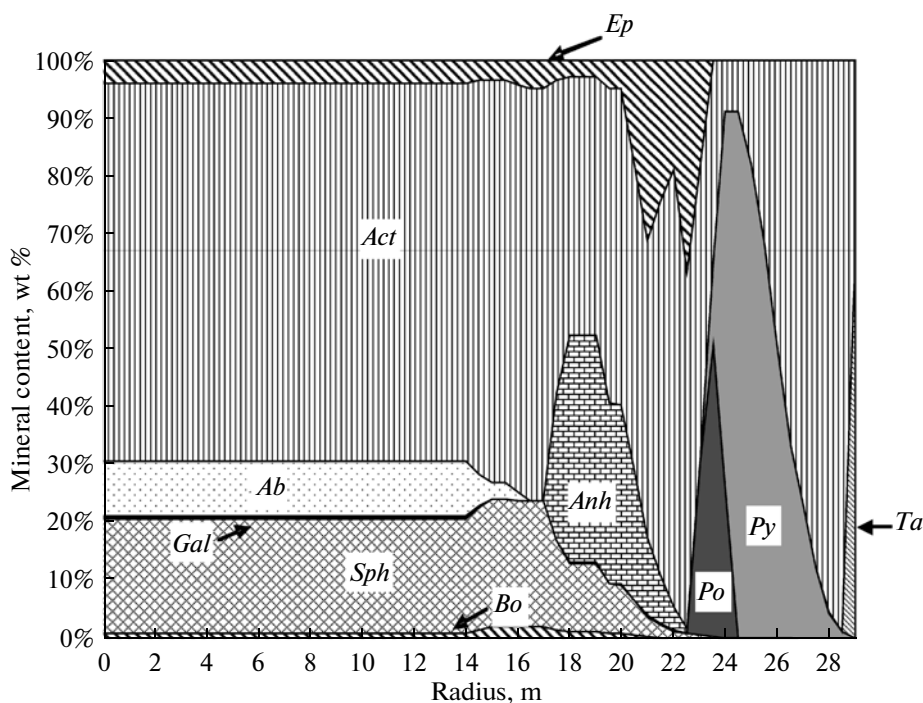


Fig. 7. Variation in the mineral composition of the simulated orebody in its radial section.

Simulation parameters: basalt as the host rock, $R/W = 1$, $T_{\max} = 370^{\circ}\text{C}$, flow rate 100 kg/s, 100th time step, step duration = 10^9 s, the system is assumed to be metastable with respect to the sulfate-sulfide reaction.

Mineral symbols: *Ep*—epidote, *Act*—actinolite, *Ab*—albite, *Anh*—anhydrite, *Py*—pyrite, *Po*—pyrrhotite, *Gal*—galena, *Sph*—sphalerite, *B*—bornite, *Ta*—talc.

Our simulations indicate that practically identical assemblages of metasomatic minerals replace all types of arc rocks. When the effect of water is predominant, the mineral assemblages include chlorite + kaolinite + quartz + hematite + anhydrite (assemblage 1). If the effect of rocks is predominant, the chlorite + actinolite + epidote + albite + sericite + quartz assemblage is formed (assemblage 2). An illustrative example of the distribution of minerals along the flow line of the solution is presented in Fig. 8. This character of the interaction of seawater with rocks is generally analogous to our earlier results on hydrothermal systems in mid-oceanic ridges with tholeiitic crust [1, 19].

Chalcophile ore elements completely pass into solution when assemblage 1 is stable but can form sulfides when in contact with assemblage 2, and the mobility of these metals is then limited. This is an important feature of the hydrothermal systems in question and plays a decisive role in understanding their geochemistry.

Being in equilibrium with analogous assemblages, the solutions have a generally similar major-component composition in variants of the model with different rocks at the same temperature, pressure, and rock/water (R/W) ratio. The variations in the composition of the generated hydrothermal solutions relative to the original seawater is given in a general form in

Table 5. An important difference was found for typical rocks of island arcs: the lower Ca and Fe(II) concentrations in these rocks cause the better preservation of seawater sulfates in the solution compared to the variant with MORB, and these sulfates are not as actively precipitated in the form of anhydrite or are reduced to H_2S .

The buffer capacity with respect to the effect of seawater is generally much lower for acid rocks than for tholeiitic and calc-alkaline basalts, and this results in a more rapid evolution of island arc hydrothermal systems from the rock-dominated to fluid-dominated regime. A possible indicator of this evolution is the rock/water (R/W) ratio at which the metasomatic assemblages are changed.

Figure 9 summarizes the results on all rock types and demonstrates that the rocks can be arranged in the following sequence according to the R/W coordinates of the boundary between their assemblages 1 and 2: MORB (20 g/kg of solution) < calc-alkaline basalt (25 g/kg of solution) < andesite (34 g/kg of solution) < dacite (39 g/kg of solution) < rhyolite (52 g/kg of solution).

This dependence is of crucial importance for the evolution of hydrothermal systems. The higher the R/W ratio required for the change in the assemblages, the sooner this change occurs during water convection in the system. As follows from our earlier results on

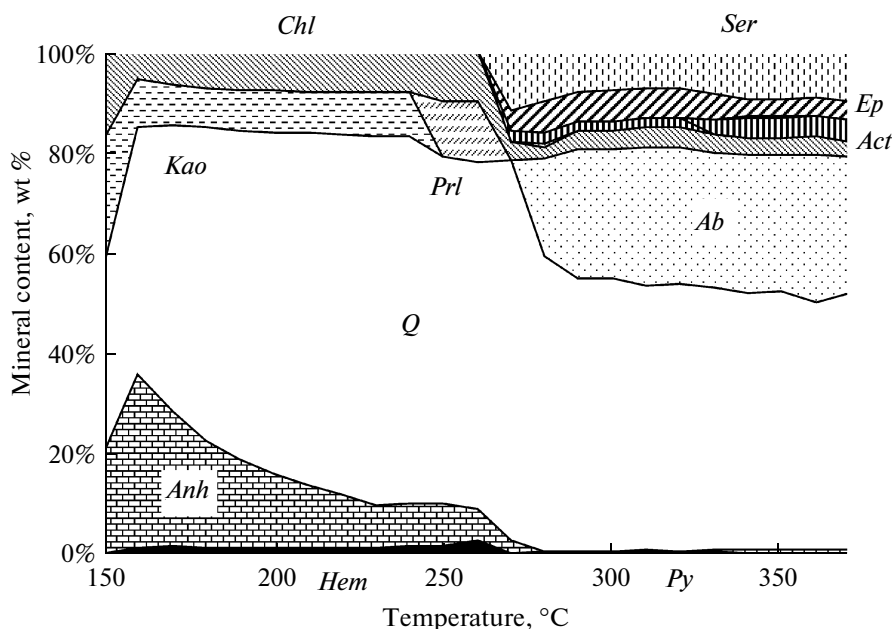


Fig. 8. Distribution of metasomatic minerals along the flow line of solution in the descending branch of the hydrothermal system. Model with andesite as the host rock. Simulation parameters: $R/W = 1$, $T_{\text{max}} = 370^\circ\text{C}$. Mineral symbols: *Ser*—sericite, *Ep*—epidote, *Act*—actinolite, *Chl*—chlorite, *Ab*—albite, *Kao*—kaolinite, *Prl*—pyrophyllite, *Q*—quartz, *Anh*—anhydrite, *Hem*—hematite, *Py*—pyrite.

simulating hydrothermal systems in mid-oceanic ridges [1, 19], the rate of metasomatic evolution within the system is closely related to the behavior of ore metals. Mature hydrothermal systems in which the front of assemblages 1 has advanced toward the high-temperature part of the system are the most productive in terms of ore material.

In order to evaluate this effect, we have simulated the evolution of hydrothermal systems in various rocks

and calculated for this the passage of 100 portions of solution through each of the rock types. The calculated production (cumulative removal) of metals in hydrothermal systems is shown in Fig. 10.

The production of metals in the system is normalized to 1 kg of solution at each calculation step. If the discharge rate of the hydrothermal system is assumed to be 100 kg/s and the calculation step is 10^9 s (close to 30 years), then the calculated variants of 100 steps cor-

Table 5. Integral characteristics of hydrothermal solutions generated during interactions with various host rocks (simulation, 370°C , 500 bar, $R/W = 1$)

| Component | MORB | basalt | andesite | dacite | rhyolite |
|----------------------|-----------|-----------|-----------|-----------|-----------|
| K | + | + | + | ++ | ++ |
| Ca | + | + | + | + | |
| Si | + | + | + | + | + |
| Fe | + | + | + | + | + |
| H ₂ S | + | + | + | + | + |
| TMe | + | + | + | + | + |
| H ₂ (mol) | 10^{-2} | 10^{-4} | 10^{-4} | 10^{-5} | 10^{-5} |
| Mg | — | — | — | — | — |
| SO ₄ | -- | -- | — | — | |
| Na | | — | — | — | — |
| pH _T | 6.0 | 5.5 | 5.5 | 5.6 | 5.6 |

Note: (+) means enrichment in solution, and (–) means depletion in solution relative to seawater (doubled signs mean that the effect is very significant).

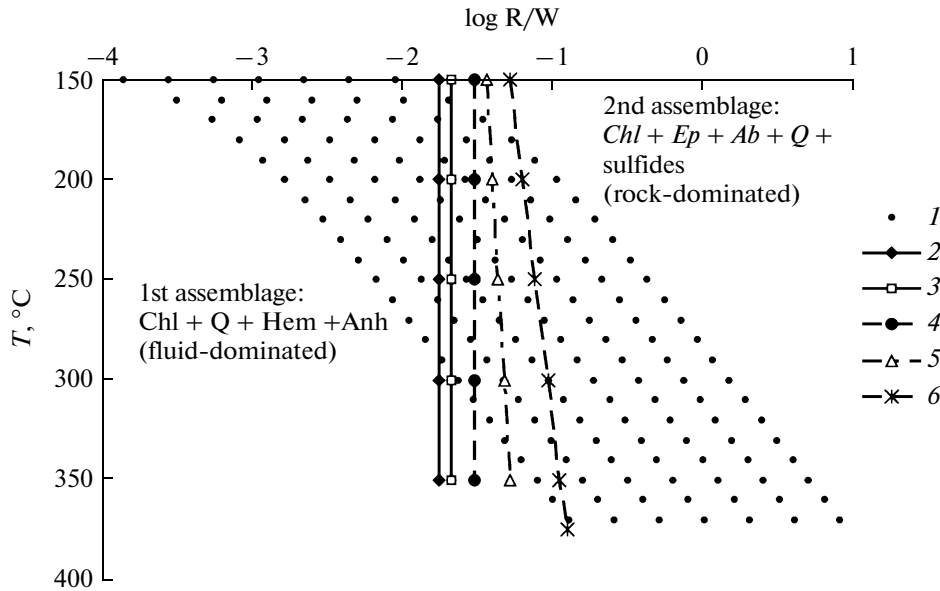


Fig. 9. Model of the descending convection branch. Boundary lines between metasomatic mineral assemblages 1 and 2 for various rock types in a temperature versus rock/water ratio diagram.

1—Simulated points, 2—MORB, 3—basalt, 4—andesite, 5—dacite, 6—rhyolite.

respond to the activity of the system over a time span close to three thousand years, and the vertical scale is million tons.

Our data indicate that island arc systems should be remarkably more productive than analogous systems in mid-oceanic ridges with respect to such major ore-forming metals as Fe, Cu, and Pb and roughly equally productive with respect to Zn.

The results of our simulations (Fig. 10) indicate that the low buffer capacity of island arc rocks causes the fairly rapid complete scavenging of base metals (Cu, Zn, and Pb). An analogous result was obtained on minor chalcophile elements (As, Sb, Ag, and Au) not shown in the figures. This has an important geochemical implication: the total fraction of these elements in the overall production of hydrothermal systems in island arcs is controlled by the abundances of these elements in the recycled rocks (and their transport with magmatic fluid, see below). This result is in good agreement with the established dependence of the metallogenic specifics of sulfide deposits on the ratios of the metals in the host rocks [55 and others].

The productivity of hydrothermal systems in terms of sulfide sulfur (Fig. 11) was proved to be remarkably lower than that in mid-oceanic ridges. This difference is due to two factors: the lower abundances of sulfide sulfur compared to those in MORB (200–380 and 800 ppm, respectively, see Table 1) and the lower ability of the circulating seawater to reduce sulfides.

The differences between rocks are the most significant in the ratio of metals to sulfide sulfur ($\text{Fe} + \text{Cu} + \text{Zn} + \text{Pb}$)/S (Fig. 12). This ratio of MORB is much

lower than one, and hence, hydrothermal solutions coming from deeper levels to mid-oceanic ridges can precipitate fairly much metals contained in them, with hydrogen sulfide remaining in excess. Such ratios are indeed detected in young high-temperature hydrothermal systems in mid-oceanic ridges. In contrast to what is simulated in the variant with MORB, hydrothermal solutions generated in island arc rocks (first of all, in acid rocks, such as rhyolite and dacite) have ratios of the metals to sulfide sulfur greater than one (Fig. 12). It is reasonable to expect that no complete precipitation of metals is possible at such ratios (which pertains first of all to Fe, which is predominant in the solutions), and the limiting factor of the ore-forming process in this situation is sulfide sulfur.

In order to test this hypothesis, we compared the results obtained on the precipitation of ore material when different host rocks of the hydrothermal systems are used (Fig. 13). These results demonstrate that, in spite of the differences in the productivity of hydrothermal systems in terms of metals (Fig. 10), the masses of ore material in these variants of the model are similar. Moreover, the smallest masses of the ore precipitate were obtained in the variant with dacite, although the production of all metals (except only Zn) in the system with dacite is greater than in the variant with MORB. The reason for this equalization is that the convective system is deficient in sulfide sulfur.

Our results exhibited in Fig. 13 show that the mineralogy of the ore precipitates also significantly varies. Although the predominant mineral in all variants is pyrite (and this is consistent with what can be seen in

naturally occurring prototypes), ore precipitates in island arcs contain much more Cu sulfides and bear sulfosalts. It should also be mentioned that the absence of sphalerite in the variant with rhyolite does not mean that the ores contain no Zn, which is accommodated in sulfosalts (Zn-tennantite) in the model.

Effect of the presence of sedimentary rocks. In contrast to mid-oceanic ridges, the crust in island arcs can contain much sedimentary rocks. Although the contribution of sedimentary material to young volcanic cones seems to be negligibly small, this factor for the slopes and calderas of submarine volcanoes should obviously be taken into account. This also pertains to troughs (such as the Okinawa Trough [8]) and ridges in island arcs.

In order to quantify the effect of sedimentary material on the ore-forming process in island arc systems, we have simulated a model that differed from that described above in involving an additional step between the chamber of the hydrothermal systems (370°C, 500 bars) and the ore deposition step (150°C, 200 bar). This additional step (350°C, 300 bars) geologically corresponds to the feeder of the hydrothermal system. We have simulated pairs of variants: the additional step contained the same rocks as the descending branch of the system in one of these variants and contained calcareous terrigenous sediments in the other. The composition of these sediments utilized in the model is presented in Table 1, and the simulation result for the variant with andesite is shown in Fig. 14.

The most important consequence of the occurrence of sedimentary rocks in the hydrothermal system turned out to be the dramatic decrease (by more than one order of magnitude) in the amount of ore material precipitated on the seafloor. Sedimentary rocks in the zone of feeder channel efficiently bind ore metals and prevent their passage to the seafloor. This effect is the most conspicuous for pyrite and Cu sulfides, whereas Zn is not as significantly precipitated in the feeder zone and can reach the seafloor surface. Because of this difference, sphalerite was proved to be an even predominant component in the variant with sediments (although its absolute mass in the "pure" andesite variant was greater, its percentage in the ore precipitate was as low as 6%). The ore material in the variant with sediments is also relatively enriched in Pb, As, and Sb, and this is pronounced in the occurrence of such minerals as galena (1%), fahlores (8%), and orpiment (1%). The reason for the differences in As and Pb is, first of all, the higher concentrations of these elements in the sediments than in andesite (Table 1). The reason for Sb concentrating (whose contents were assumed to be the same) was likely the somewhat more alkaline environment of precipitation.

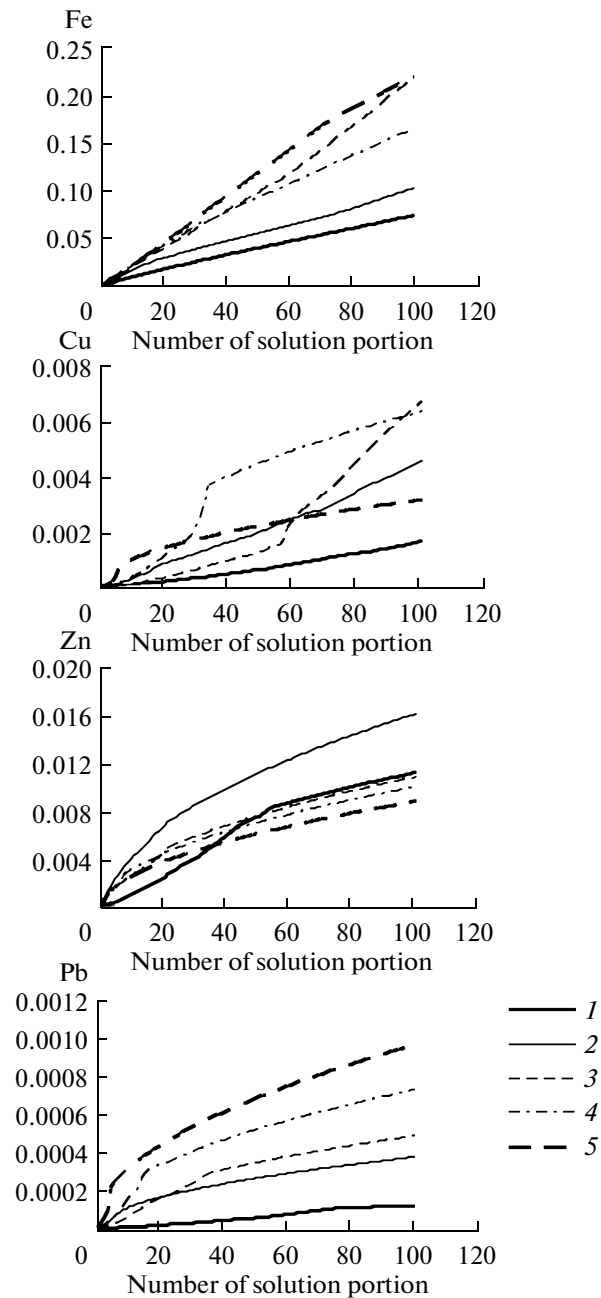


Fig. 10. Cumulative removal of metals (in mol per 1 kg/s of the flow rate of the system) from long-lived hydrothermal systems with various host rocks from which the metals are scavenged. Simulation parameters: $R/W = 1$, $T_{\max} = 370^{\circ}\text{C}$, 100 calculation steps. 1—MORB, 2—basalt, 3—andesite, 4—dacite, 5—rhyolite.

The character of interaction between hydrothermal solutions and sedimentary rocks was elucidated by simulating an additional model for the development of a metasomatic zoning in the wall-rock of her feeder. The methodology of the calculation is described in [56]. The material of sedimentary rocks is metasomatized (generally under parameters of the prehnite—

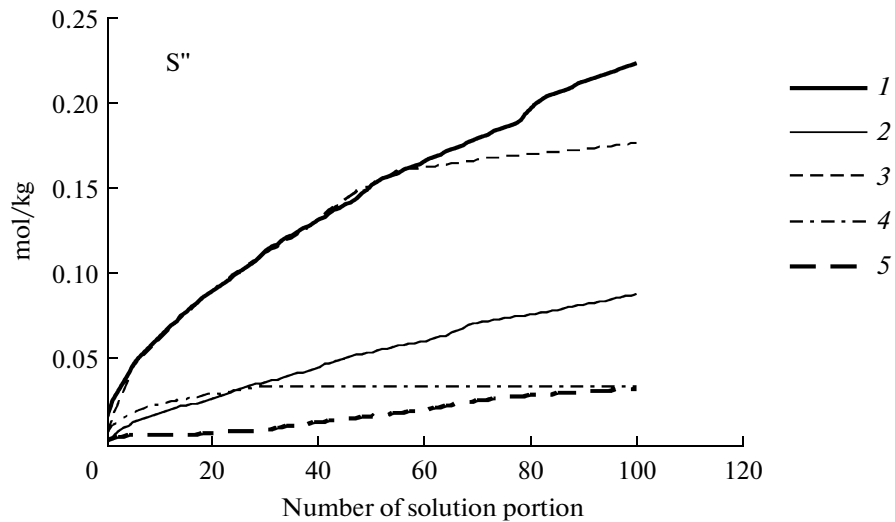


Fig. 11. Cumulative removal of sulfide sulfur (in mol per 1 kg/s of the flow rate of the system) from long-lived hydrothermal systems with various host rocks from which the element is scavenged. Simulation parameters: $R/W = 1$, $T_{\max} = 370^{\circ}\text{C}$, 100 calculation steps.

1—MORB, 2—basalt, 3—andesite, 4—dacite, 5—rhyolite.

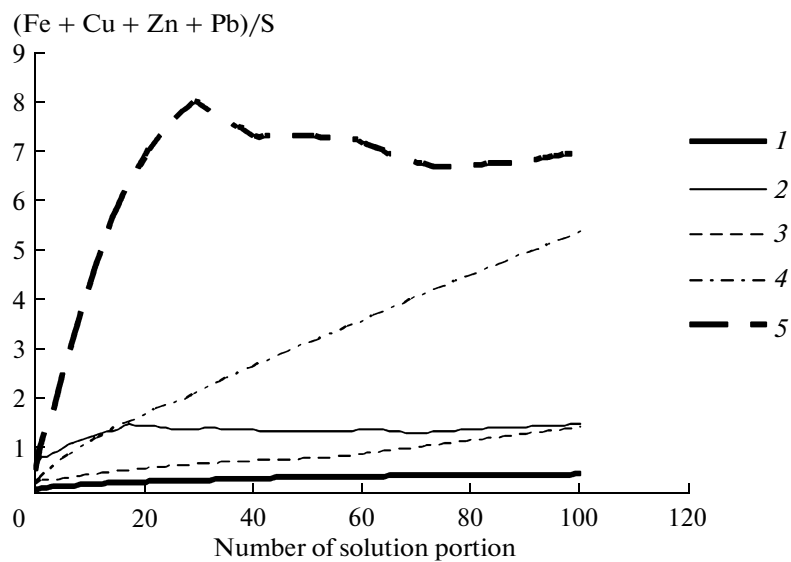


Fig. 12. Relations between the cumulative removal of metals and sulfide sulfur (mol/mol) in a hydrothermal system depending on the composition of the host rock from which the elements are scavenged. Simulation parameters: $R/W = 1$, $T_{\max} = 370^{\circ}\text{C}$, 100 calculation steps.

1—MORB, 2—basalt, 3—andesite, 4—dacite, 5—rhyolite.

pumpellyite facies) under the effect of hydrothermal solutions. The major acting component of the sedimentary rocks is Ca carbonate, which dissolves and effectively buffers the pH of the solution. If the original hydrothermal solution entering a sedimentary sequence has pH 3.8, the latter increases to 6.0 upon interaction with the rocks. It is this alkalization that most significantly hampers the migration of ore elements along the hydrothermal feeder. This effect is,

however, practically not pronounced in terrigenous rocks.

If hydrothermal solution interacts with rocks during a long enough time (100 solution portions were simulated in our model), a zone of chloritization and pyritization develops near the feeder and contains approximately 2% Zn sulfides and 1% Cu sulfides.

The results of our simulations indicate that sedimentary rocks in the zone of a channel serving for the

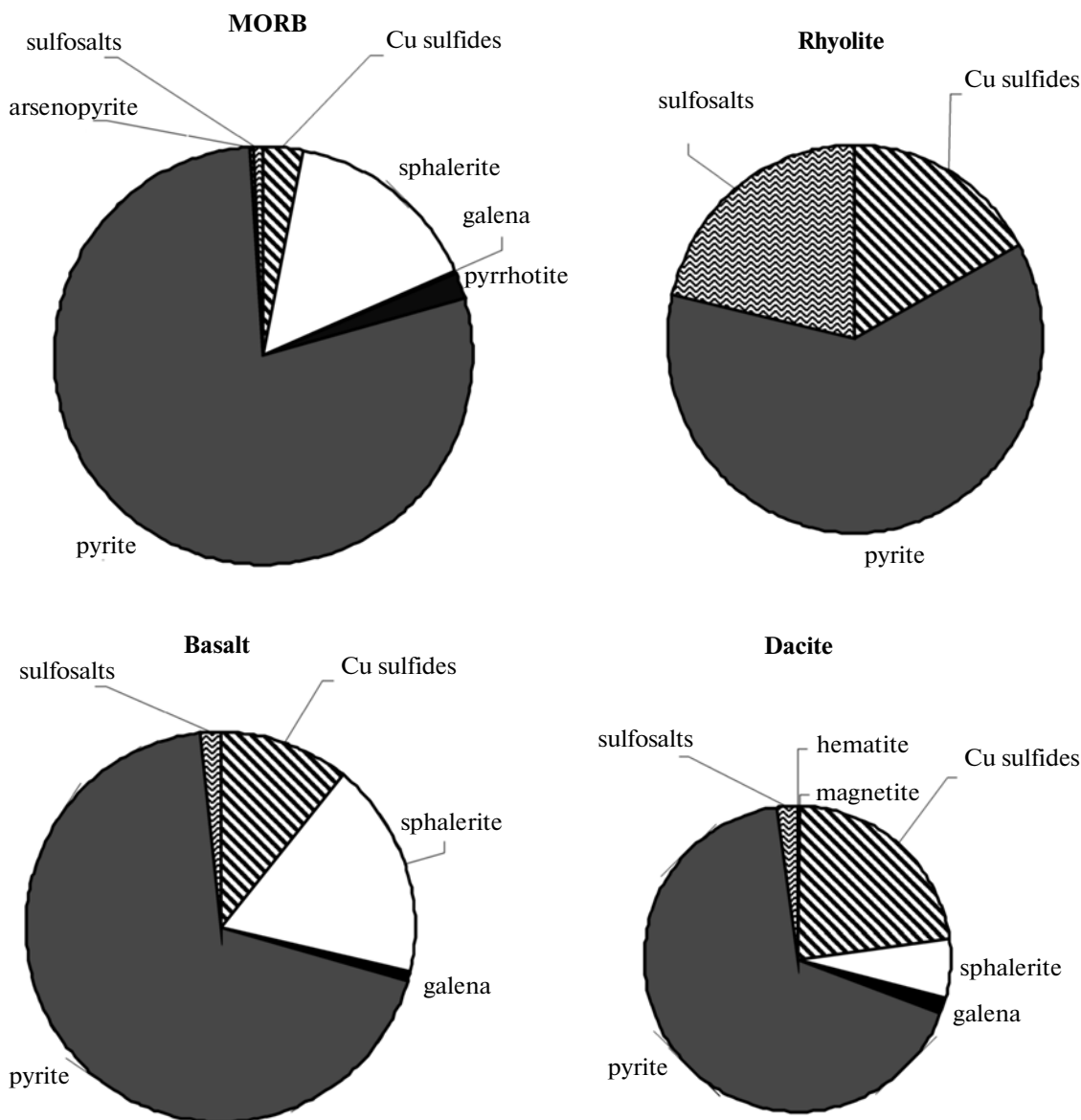


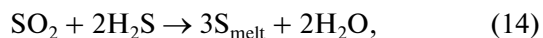
Fig. 13. Composition (wt %) of ores and the relative scale of ore precipitation in hydrothermal systems with crust of various composition. The areas of the sectors are proportional to the masses of the precipitated minerals. Simulation parameters: $R/W = 1$, ore precipitation temperature = 150°C , 100 calculation steps.

discharge of hydrothermal solutions can precipitate the bulk of the ore material contained in the solutions and thus produce disseminated and stringer ore mineralization in the metasomatized sediments. Thereby a relatively small orebody enriched in Zn, Pb, As, and Sb should be formed on the seafloor surface.

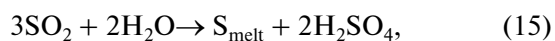
Analogous relations were also simulated for other rock types, including tholeiitic basalts. This is generally consistent with drilling data in the Middle Valley hydrothermal system [57], in which the orebody on the seafloor surface is relatively small but continues down the sediments.

Effect of magmatic fluid on the bulk composition of the orebody

As follows from our simulation results, the most reactive and unstable during cooling component of magmatic gas is SO_2 , whose behavior depends on the phase composition of the fluid. The reaction



proceeds in gas during its cooling, and the disproportionation reaction



occurs during fluid condensation or mixing with seawater.

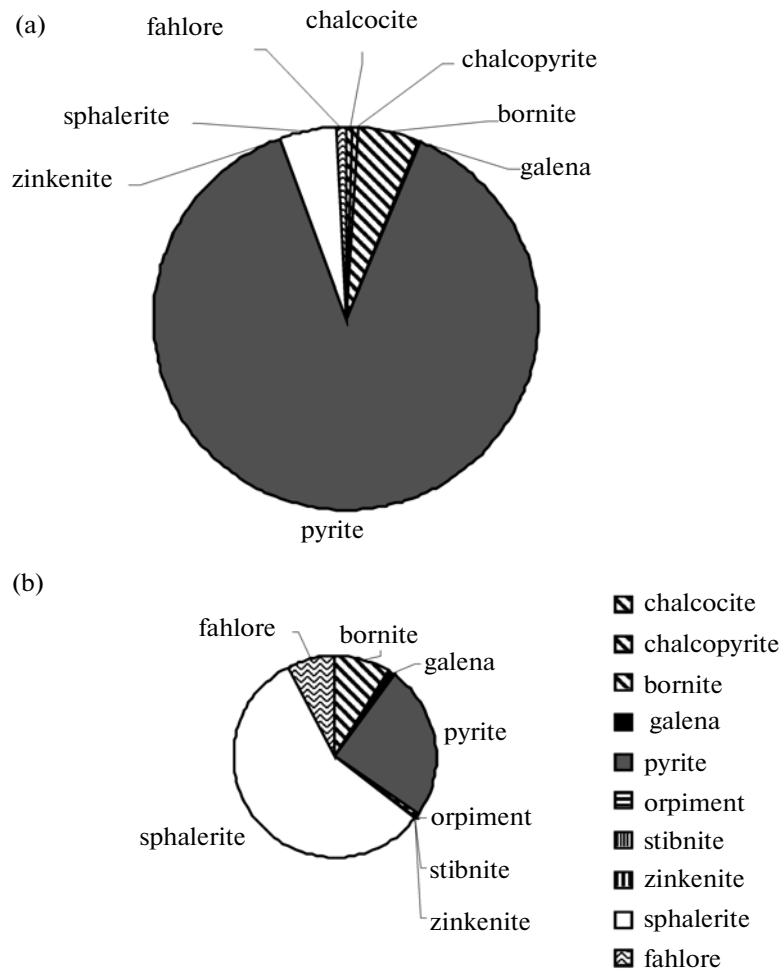


Fig. 14. Comparison of the composition (wt %) and amount of ore material precipitated at the rapid cooling of hydrothermal solutions. (a) Andesite model without sediments; (b) andesite model with sediments of calcareous terrigenous composition. The areas of sectors are proportional to the masses of the precipitated minerals. Simulation parameters: $R/W = 1$, $T_{\max} = 370^{\circ}\text{C}$, $T_{\text{ore precipitation}} = 150^{\circ}\text{C}$, 100 calculation steps.

The latter reaction significantly acidifies the solution, which becomes aggressive with respect to rocks. This effects are well known and were monitored at active volcanoes and on-land hydrothermal solutions (see, for example, [58]).

The simulation of the cooling of the magmatic fluid after introducing a correction for the degassing pressure (Fig. 3) indicate that the predominant component of the precipitate should be native sulfur (Fig. 15), whose amount directly depends on the SO_2 fraction and the character of the reaction. The reason for maximum in Fig. 15 stems from the fact that reaction (14) in fluid with a low fraction of SO_2 proceeds until SO_2 is completely exhausted, whereas this reaction in fluid with a higher SO_2 fraction proceeds until H_2S is exhausted.

Major and ore elements contained in the magmatic gas are concentrated upon its cooling and form the

mineral assemblage quartz + diaspore + anhydrite + alunite + pyrite + sphalerite + enargite + orpiment + sulfosalts (minerals are listed in descendent order of their concentrations).

The inflow of such fluid into a hydrothermal system results in a drastic change in the composition of the precipitated ore material. As an illustrative example, Fig. 16 shows the composition of hydrothermal precipitate simulated in one of the variants of the model with a mixed (recycling and magmatic) feeding. In this example, the predominant components of the hydrothermal precipitates are native sulfur, silica, anhydrite, and pyrite, whereas the crystallization of base-metal sulfides is suppressed by the high acidity of the mix solution. The acidity of the discharged solution is controlled by the addition of magmatic gas. For instance, our simulations with variable amounts of magmatic fluid “from a shallow depth” (one of the

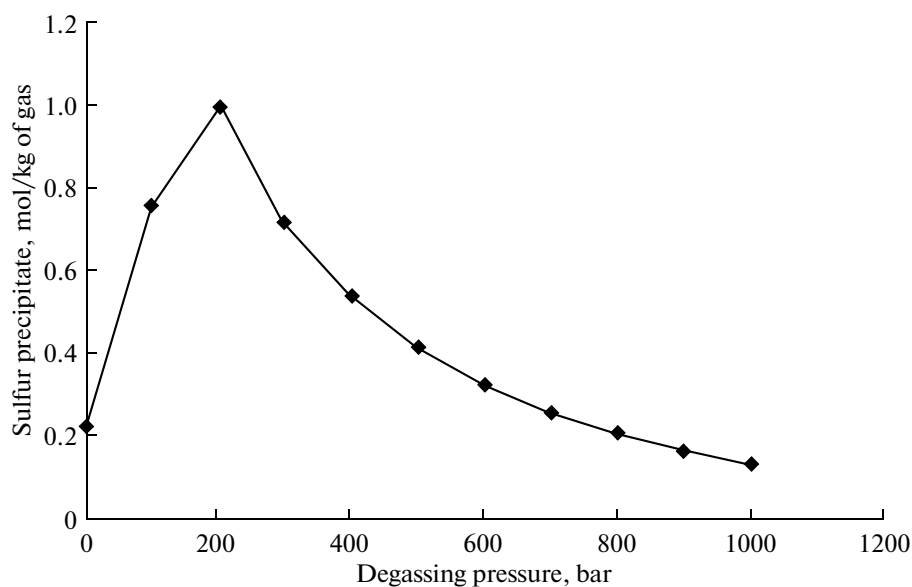


Fig. 15. Amount (mol/kg of gas) of native sulfur precipitated at the cooling of magmatic gas depending on the degassing pressure of the magma. Thermodynamic simulation. Degassing conditions: $T = 1000^{\circ}\text{C}$, $QFM + 1$ buffer; precipitation conditions: $T = 150^{\circ}\text{C}$, $P = 5$ bars.

variants is displayed in Fig. 16) yield the following dependence:

| | |
|---|------|
| pH when no magmatic gas is added | 3.0, |
| pH when magmatic gas is added in the proportion 1 : 100 | 2.6, |
| pH when magmatic gas is added in the proportion 1 : 10 | 2.5, |
| pH when magmatic gas is added in the proportion 1 : 1 | 1.3. |

Since magmatic gas ascending to the surface can react with ambient rocks and its acidity can somewhat diminish, we have simulated an auxiliary problem of magmatic gas neutralization by ambient rocks. The calculations were made for 350°C , 500 bars for magmatic gas that separated from magmatic melt at 500 bars and for 250°C , 50 bars for magmatic degassing at 100 bars. The calculations were carried out in two variants: for calc-alkaline basalts and rhyolites as the country rocks. The results indicate that the neutralization of 1 kg of gas from “deep levels” to $\text{pH} > 3$ (which is sufficient for the precipitation of base metal sulfides) requires the addition of as little as 40 g of basalt or 90 g of rhyolite, and analogously, the neutralization of 1 kg of gas from “shallow depths” requires 80 and 180 g of these rocks, respectively. This implies that the most adverse effect of magmatic gases should be expected for systems fed from shallow-sitting chambers and operating in acid rocks.

At the same time, the inferred sulfur deficit in hydrothermal systems developing in acid rocks suggests that the effect of magmatic gases on the ore-forming process in hydrothermal systems in island arcs is even more complicated and ambiguous.

This factor was estimated more accurately by simulating a model in which the mixing proportions of modified seawater, which had passed through heated rocks and enriched in metals, and magmatic fluid coming to the ore precipitation zone were broadly varied. Figure 17 shows the results of our simulations for a hydrothermal system with rhyolite in which magmatic gas is introduced in amounts from 0 to 100% of the discharge of the convective seawater flow.

At given parameters of the model in a system to which no magmatic gas was added, the ore precipitate consisted of pyrite, Cu sulfides, and sulfosalts. The addition of even minor amounts (a few tenths of a percent) of magmatic gas to the hydrothermal system remarkably enhanced sulfide precipitation. Thereby the mass of the sulfide precipitate increased by almost one order of magnitude, first of all, due to pyrite, and the precipitate contains galena and sphalerite.

A further increase (to $>1\%$) of the added amount of magmatic gas does not change the total mass of the sulfides, but the proportions of base metal sulfides change: at a high fraction of magmatic gas (1 : 1), base metal sulfides give way to sulfosalts. Thereby the non-metallic constituent of the precipitate is dominated by native sulfur (up to 90%).

Our results testify that the insignificant involvement of magmatic fluids in the hydrothermal process significantly enhances the ore-generating potential of the hydrothermal systems in acid rocks with a deficit in sulfide sulfur. A further increase in the percentage of magmatic gas results in the dilution of the ore material by pyrite and native sulfur and the transformation of

the ore-forming process from the precipitation of massive sulfides to exhalative sulfur ores.

Effect of the involvement of magmatic fluid on the structure of the growing orebody

We have also simulated a model with a hybrid scenario according to which a orebody of hydrothermal precipitates develops in two stages: (1) during the first stage (100 calculation cycles), the hydrothermal system is fed by magmatic fluid and (2) then “is switched” to seawater feeding. This scenario corresponds to the reproduced evolution of hydrothermal systems in the caldera of Brothers submarine volcano in the Tonga-Kermadec arc [12].

Figure 18 shows our simulation results: Fig. 18a exhibits the zonal structure of the orebody late during the magmatic stage (100 steps), and Fig. 18b displays this for stage 2, after further 100 calculation steps, with feeding by convecting seawater. For comparison, Fig. 18c shows a vertical section through the orebody at a partially convective feeding of the system, after 200 calculation steps.

During the magmatic stage, the orebody is large (its radius is greater than 100 m). Its central part consists mostly of pyrite, the intermediate zone of the edifice is composed of silica, and the periphery is made up of native sulfur. The volume of this peripheral zone accounts for almost half of the volume of the whole edifice. Note that native sulfur was lately found in several hydrothermal systems in island arcs (Fig. 1).

The overprinting of convective feeding onto an orebody that was produced by magmatic fluid results in the restyling of its zoning. Much anhydrite appears in the intermediate zone, and the peripheral zone with native sulfur disappears and thus “diminishes” the overall size of the body. The total mass of sulfide material in the orebody increases by a factor of 2.5, first of all, because of the development of a pyrite-bearing zone in the peripheral portion of the body. This zone was determined to contain sphalerite accumulations.

It is interesting to compare the simulated orebody that has a combined feeding with a body produced by the same volume of hydrothermal solution of convective nature (Fig. 18c). Our simulation results indicate that magmatic fluid can bring much more sulfide sulfur into the orebody, and the masses of pyrite in the variants shown in Figs. 18a and 18b are much greater than that in Fig. 18c. At the same time, the system with magmatic feeding was proved to have a zero productivity in terms of base metal sulfides, first of all, Zn and Pb sulfides.

Effect of the depth of the ore precipitation zone

The depths at which hydrothermal ore-forming processes proceed were studied for a years, and pio-

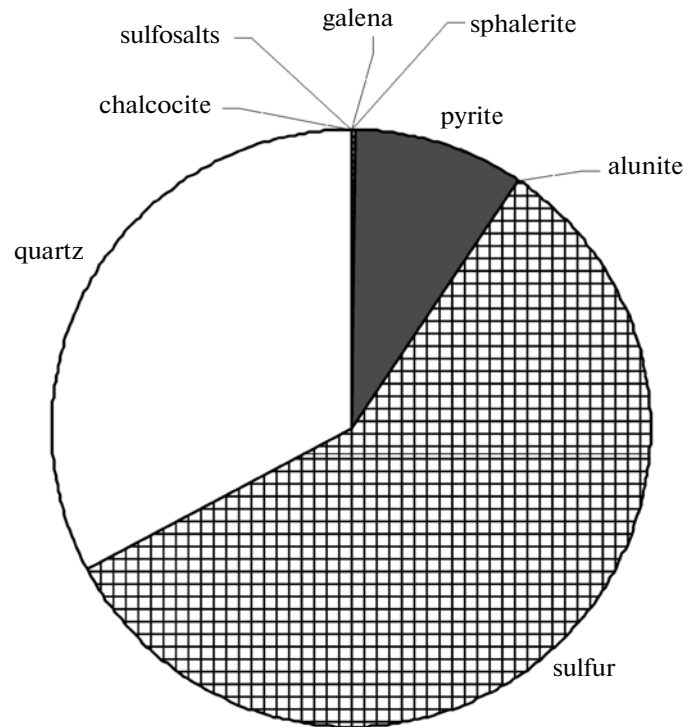


Fig. 16. Composition (%) of the precipitated material at the combined (recycling + magmatic) feeding of the hydrothermal system. Simulation conditions: rhyolite as the host rock, $R/W = 1$, $T_{\max} = 370^{\circ}\text{C}$, magmatic fluid degassing at a pressure of 100 bars, magmatic fluid in amount of 10% of the convective solution, the mixture rapidly cools to $T = 150^{\circ}\text{C}$, $P = 50$ bars, 100 steps of precipitate accumulation is simulated.

neering results were obtained by Ridge [59], who was the first to examine physicochemical data on the boiling of mineralized waters and to suggest that boiling constrains the possible range of $T-P$ parameters suitable for the precipitation of ore mineralization. The further investigation into this problem led some researchers, including Krasnov [60], to regard boiling as a factor limiting the temperature of hydrothermal solutions under a given hydrostatic pressure (i.e., seawater depth). Inasmuch as the transport of ore metals is thought to be directly controlled by temperature, this estimates provided a limit for depths, with no ore-forming processes thought to be possible at shallower water depths. Evaluations made by various researchers for the limiting depth at which massive sulfides can be precipitated range from 0.3 to 1.5 km. This constraint was generally insignificant for ore mineralization in mid-oceanic ridges because the depths of the overwhelming majority of hydrothermal fields found so far are greater than 1.5 km. The situation with island arcs is, however, principally different. Although hydrothermal fields in interarc troughs were found at significant depths (such as the Archaean Site in the Mariana Arc), most of the currently known hydrothermal fields

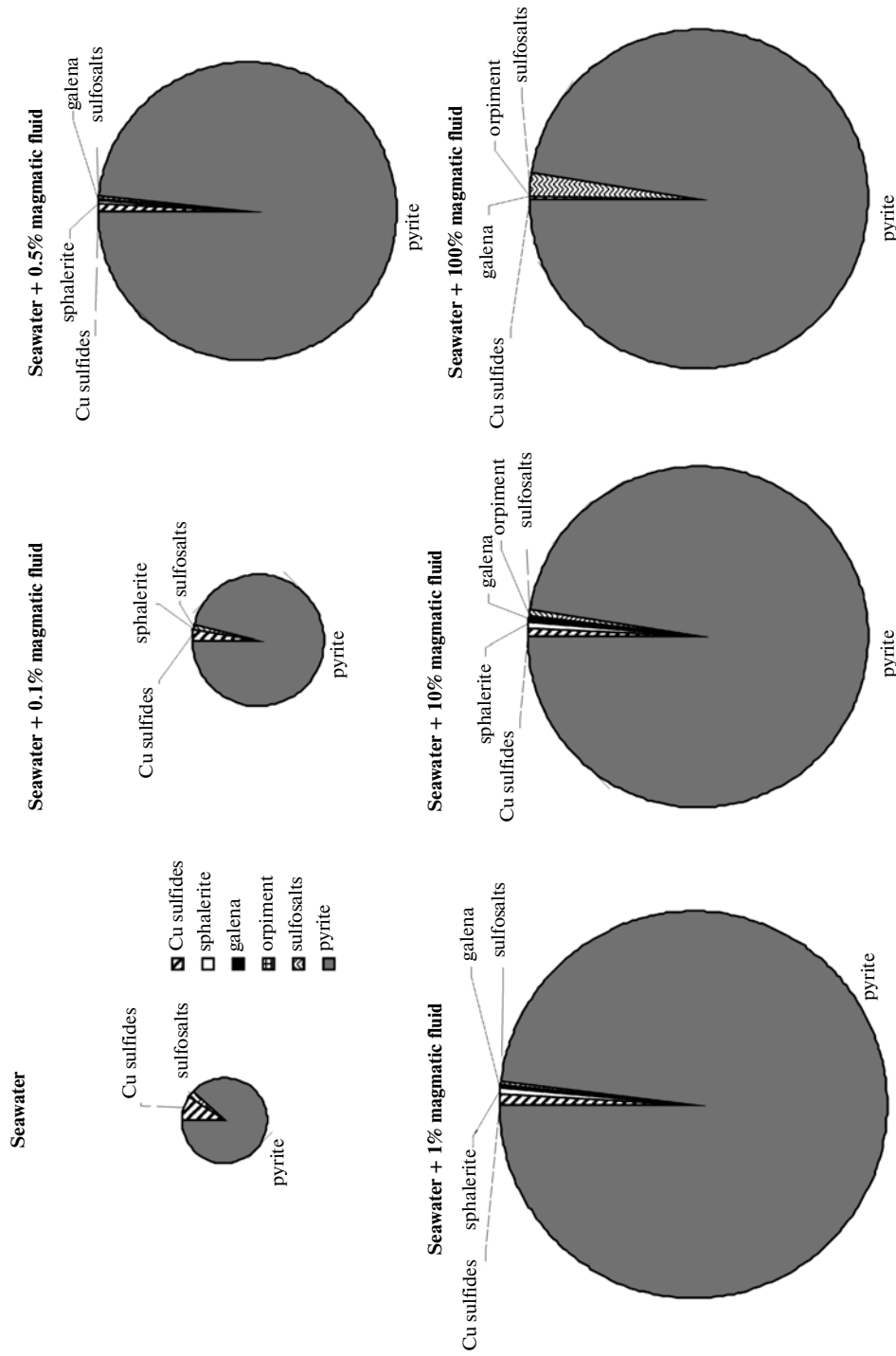


Fig. 17. Effect of the amount of added magmatic fluid on the ore-forming process in an arc hydrothermal system. Thermodynamic simulation. Simulation conditions: rhyolite as the host rock, $R/W = 1$, $T_{max} = 370^{\circ}C$, magmatic fluid degassing at a pressure of 100 bars, the mixture rapidly cools to $T = 150^{\circ}C$, $P = 50$ bars, 100 steps of precipitate accumulation is simulated. Sulfide components of the ore precipitates are shown, the areas of sectors are proportional to the masses of minerals.

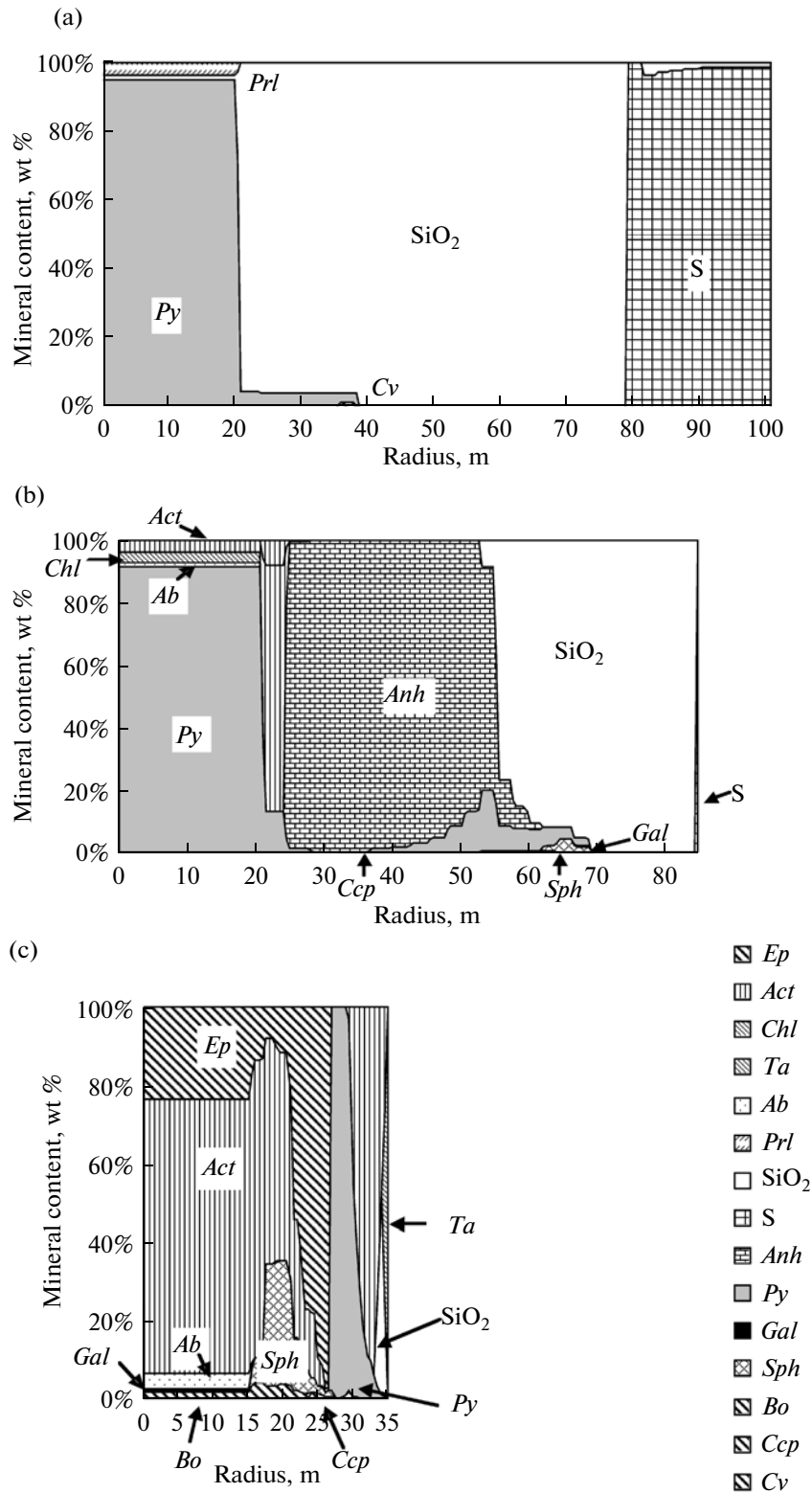


Fig. 18. Mineral composition in a radial section of a simulated orebody with combined feeding. Simulation conditions: basalt as the host rock, $R/W = 1$, $T_{max} = 370^{\circ}C$, flow rate of the system is 100 kg/s, simulation step is 10^9 s.

Stage 1: the system is fed exclusively by magmatic fluid, 100th simulation step;

Stage 2: starting with step 100 until step 200, the system is fed by convecting seawater;

Stage 3: the system is fed exclusively by convecting seawater, 200th simulation step.

Mineral symbols: *Ep*—epidote, *Act*—actinolite, *Chl*—chlorite, *Ta*—talc, *Ab*—albite, *Prl*—pyrophyllite, SiO_2 —amorphous silica, *Anh*—anhydrite, *S*—sulfur, *Py*—pyrite, *Ccp*—chalcocopyrite, *Bo*—bornite, *Sph*—sphalerite, *Gal*—galena, *Cv*—covellite.

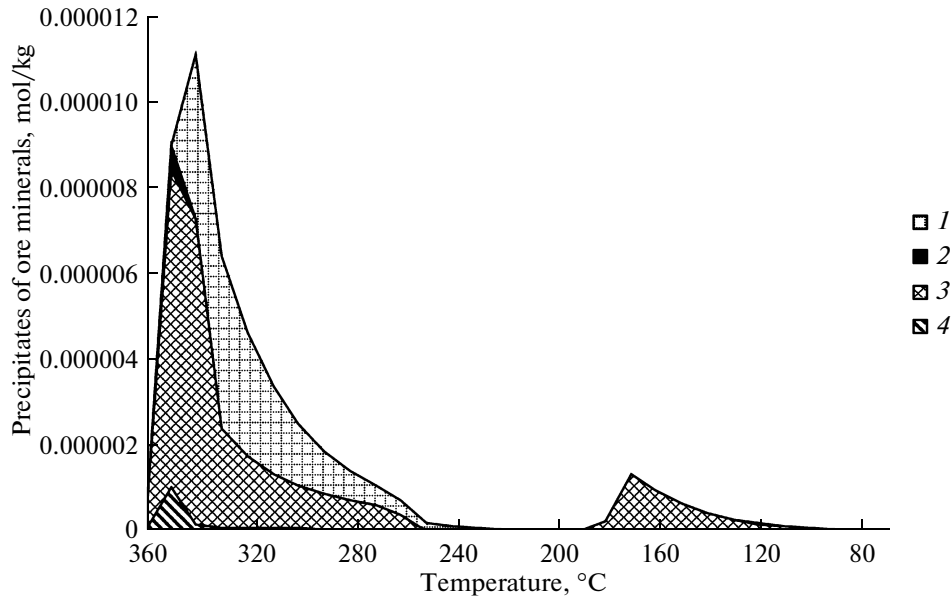


Fig. 19. Precipitation of sulfides at fluid cooling along the water boiling curve to a pressure of 50 bars. The mass of the precipitate is normalized to 1 kg of the discharged hydrothermal solution.

Simulation conditions: andesite as the host rock, $R/W = 1$, $T_{\max} = 370^{\circ}\text{C}$, temperature at the channel mouth is $T = 260^{\circ}\text{C}$ (seawater depth is close to 500 m). Any fluid portion is assumed to be a closed system.

Minerals: 1—arsenopyrite, 2—galena, 3—sphalerite, 4—chalcopyrite (the precipitation of pyrite, pyrrhotite, and quartz is not shown).

in arcs occur at depths of 1 to 2 km, and this makes the problem of the limit for the depth of hydrothermal ore-forming processes crucially important (see, for example, [60]).

In our earlier publication [19], it has been demonstrated that the boiling of hydrothermal solutions is associated with a significant redistribution of components between the solution and vapor phases, for instance, the transfer of H_2S into vapor. This redistribution increases the solubility of sulfides in boiling fluids and enhances the transport capability of the latter. In other words, if certain elements are precipitated in form of sulfides and are not transported in the form of hydrosulfide complexes (which are Fe, Cu, Zn, Pb, and also perhaps Ag, Sb, and As in oceanic hydrothermal systems), fluid heterogenization is favorable for the transport of these metals and correspondingly leads to an increase in the temperature range within which the transfer of ore metals remain efficient and, hence, decrease the limiting seawater depth at which ore mineralization can be deposited. This conclusion should be specified in terms of both the list of elements to which it pertains and the quantitative evaluations.

With regard for the compositional specifics of hydrothermal systems in island arcs, we carried out thermodynamic simulations of the transport of ore-forming elements with boiling hydrothermal solutions during the cooling of the latter. The model was simulated for the following assumed conditions: the hydrothermal solution is generated in a system with rhyolite

at $T_{\max} = 370^{\circ}\text{C}$, $P = 500$ bars, and $R/W = 1$ kg/kg (by analogy with the models discussed above). The solution then ascends to the surface and boils at a temperature of 350°C and pressure of 161.5 bars in contact with rock. The further decrease in the hydrostatic pressure is associated with the adiabatic cooling of the vapor-bearing aqueous fluid according to the isoenthalpic law.

The simulation of the adiabatic boiling of the hydrothermal solution was conducted with the HCh program package at a temperature step of 50°C and the pressure determined by the technique described in [19]. The temperature–pressure pairs at discrete calculation steps were as follows: 300° and 82.3 bars, 250° and 38.6 bars, 200° and 15.05 bars, and 150° and 4.59 bars, which roughly corresponds to depths of cold seawater of 820, 380, 150, and 46 m. In contrast to our earlier simulations [1, 19], this model was simulated with regard for the nonideality of the vapor phase, which was modeled by the modified Peng–Robinson equation (PRSV2).

We have also simulated a variant with phase separation, i.e., the irreversible separation of the vapor phase from the aqueous solution, as is thought [6 and others] to take place in modern oceanic hydrothermal systems; this corresponds to the Rayleigh exhaustion of the components more readily transferred into vapor. According to earlier evaluations [19], this process should be more favorable for the transport of chalcop-

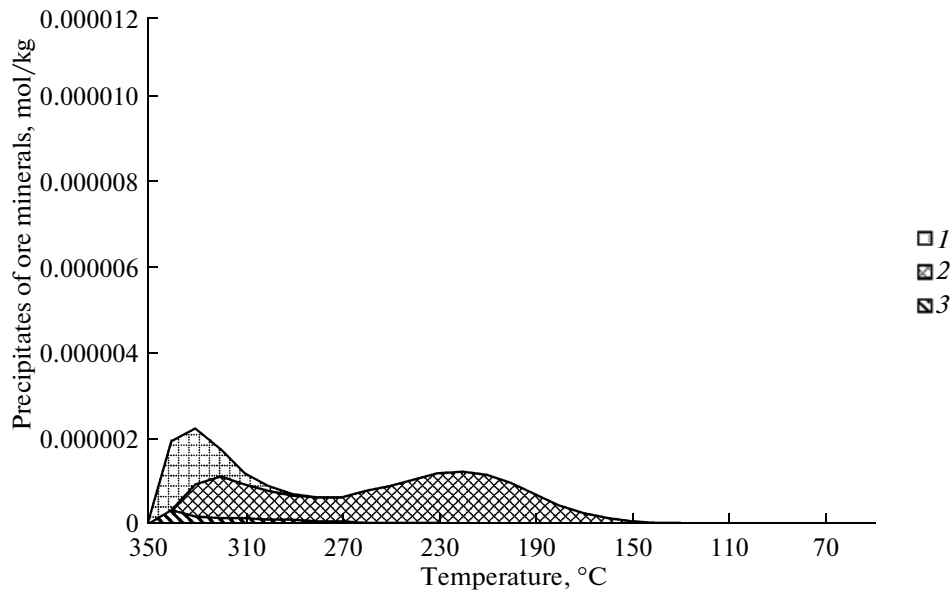


Fig. 20. Precipitation of sulfides at the phase separation of gas. The mass of the precipitate is normalized to 1 kg of the discharged hydrothermal solution.

Simulation conditions: andesite as the host rock, $R/W = 1$, $T_{\max} = 370^{\circ}\text{C}$, phase separation starts at $270^{\circ}\text{C}/210$ bars and ends at $80^{\circ}\text{C}/115$ bars.

Minerals: 1—arsenopyrite, 2—sphalerite, 3—chalcopyrite (the precipitation of pyrite, pyrrhotite, and quartz is not shown).

phile elements because of the loss of sulfide sulfur as the precipitating agent.

Simulations in a closed system are exhibited in Fig. 19 and indicate that boiling in a closed system cannot prevent the precipitation of chalcophile elements: Cu, Zn, Pb, and As are mostly precipitated at temperatures higher than 300°C , and only minor amounts of these elements can remain in the solution throughout this temperature range and be deposited at the seafloor.

The situation is, however, different if the mechanism of Rayleigh exhaustion operates with respect to sulfide sulfur (Fig. 20). The temperature range remains the same for Cu and As, but more than half of Zn passes through it and is precipitated at temperatures of $230\text{--}190^{\circ}\text{C}$, which corresponded to boiling depths as shallow as $300\text{--}150$ m.

Silver is precipitated in a boiling closed system in the form of argentite at temperatures of 200°C and lower, and still lower temperatures are required for the precipitation of gold: $160\text{--}110^{\circ}\text{C}$. Paradoxically, Ag is precipitated in an open system at a higher temperature than in a closed one, and its precipitation mode is native metal. This corresponds to hydrogen sulfide loss from the solution, but the precipitation of native silver requires more reduced conditions.

The low temperatures at which Ag, Au, and Sb are precipitated in the boiling model are consistent with currently available information on oceanic hydrothermal systems [61 and others]. At the same time, our

simulation results still cannot be considered final because our model does not fully take into account the precipitation of minor chalcophile elements as isomorphic components (Ag in galena and sphalerite, Au and As in pyrite, etc.), and isomorphism of minor elements remarkably complicates our simulation results.

Our simulation results led us to conclude that temperature constraints imposed onto the transfer of metals with boiling fluids turned out to be not as strict as was thought previously because of H_2S redistribution between phases. The critical depth of precipitation is close to 1 km only for Cu and is greater than 0.5 km for As, whereas the effective transfer of Zn, Pb, Sb, and Au with heterogeneous fluid is possible to depths of $150\text{--}200$ m. Thus, there are no physicochemical limitations for the generation of sulfide orebodies at shallow seawater depths, and these environments are unfavorable only for the focused precipitation of Cu.

Discussion of simulation results

1. One of the principally important results of our simulations is the conclusion that the proportions of ore-forming metals in the ores of island-arc hydrothermal systems inherit the ratios of the abundances of these elements in the host rocks, with a correction for the addition of As and Sb with the magmatic fluid. Our simulations indicate that this inheritance should be pronounced in hydrothermal systems in island arc more clearly than in those in MOR, in which Zn and Cu are often differentiated [19]. With regard for avail-

able data on the abundances of elements, ores in arc systems should be richer in Pb, As, and Sb but contain comparable concentrations of Zn and Cu. Extensive observations still do not provide sufficient information to reliably estimate the composition of submarine sulfide ores in island arcs. At the same time, currently available data suggest that arc ores should be enriched in As, Sb, Pb, Ag, and Hg ([29, 62, 63, and others]).

2. The assemblages of major ore-forming minerals in arc hydrothermal ores are generally the same as in widely known sulfide ores in MOR: pyrite, sphalerite, chalcopyrite, and bornite in association with anhydrite and silica. The model for arc hydrothermal systems differs in the presence of native sulfur (see below) and the absence of pyrrhotite. The differences between the assemblages of minor minerals are more conspicuous. Arc ores in the model sometimes contain orpiment and enargite, which are atypical of ores in MOR, and relatively high concentrations of galena, fahlores, and Ag sulfosalts. These features were persistently documented in hydrothermal ore mineralization in island arcs [29, 62, 64, and others].

3. As was demonstrated in our earlier publications, a distinctive feature of hydrothermal solutions fed (at least during their early evolution) by magmatic fluids is the pronounced metasomatic alterations of the wall rocks around the hydrothermal feeder beneath the ore mineralization [65]. Conversely, massive sulfide ores in mid-oceanic ridges typically do not show any metasomatic zoning around the feeders, and the metasomatic alterations are poorly pronounced and involve chloritization, pyritization, silification, and the development of paragonite [66].

Our simulation of the effect of magmatic gas (this publication) on the ambient rocks indicates that the alterations of these rocks should be constrained to their very significant acidic leaching. The resultant mineral assemblage quartz + pyrite ± diasporite ± pyrophyllite ± ... corresponds to secondary quartzite in Russian geological terminology and to the advanced argillic alteration, as it is conventionally referred to by western geologists. The occurrence of alunite and anhydrite in the ore precipitation zone corresponds to the high sulfidation, which is typical of metasomatism at epithermal volcanic gold deposits [67 and others].

Lately obtained data indicate that this exactly type of alterations of country rocks is typical of hydrothermal solutions in island arcs with evidence of magmatic feeding: PACMANUS and Onsen in the Manus Basin, Hine Hina in the Lau Basin, young volcanic cone in the caldera of Brothers submarine volcano in the Kermadec arc, cones of submarine volcanoes in the Mariana Arc, and some other hydrothermal solutions [12, 24, 28, 68, 69, and others].

4. The fairly unusual composition of hydrothermal solutions in systems involving magmatic fluid, such as

elevated acidity (pH up to 1), elevated concentrations of sulfates, and precipitation of native sulfur, is completely reproduced in our model simulations. Naturally occurring hydrothermal systems exhibit even such minor features as high concentrations of hydrogen sulfide in hydrothermal solutions discharged at significant depths (hydrothermal fields PACMANUS [23, 25] and others) and very low hydrogen sulfide concentrations in hydrothermal vents at shallow water depths (NW Rota-1 volcano [26]).

5. The precipitation of native sulfur in hydrothermal solutions (not related to bacterial processes) was identified so far at no less than 25 hydrothermal fields in the island arcs Okinawa, Izu-Bonin, Mariana, Tonga-Kermadec, Bransfield, Hellenic arc, and in the Lau and Manus basins (Fig. 1). Sulfur-bearing hydrothermal systems found so far occur at seawater depths of 0–2 km (Fig. 21), but the reportedly most significant occurrences of native sulfur in the Mariana arc occur at depths of 400–550 m. Ponds and flows of molten sulfur were thereby found at young cones of submarine volcanoes in the Mariana arc, and sulfur permeates volcanic and hydrothermal sediments at other volcanoes [13, 70–72, and others].

Isotopic composition of sulfur proves that elementary sulfur can precipitate in hydrothermal systems in island arcs as a consequence of the disproportionation of magmatic SO₂ [23, 24, 73, 74, and others].

According to our model, the precipitation of elementary sulfur is antagonistic towards the precipitation of massive sulfide ores with high contents of base metals.

Observations at naturally occurring hydrothermal systems indicate that most of these systems with elementary sulfur have no sulfide edifices [13, 71, and others]. It is thus interesting to consider instances when the precipitation of sulfur and sulfide was detected within a single hydrothermal system (cluster of hydrothermal vents). Three such systems are described in much detail in the literature.

A) Discharges of hydrothermal solutions in the caldera of submarine Brothers volcano [12, 28]. A field with deposited native sulfur was discovered at the young cone of this volcano, and a large sulfide hydrothermal edifice with active black smokers occurs on the northwestern wall of the caldera. Scientists who examined the edifice believe that its sulfur and sulfides differ in age: a young hydrothermal system with magmatic feeding developed at the young cone, and an older system that is now fed with seawater sits in the caldera. Note that this evolutionary scheme of the hydrothermal system is completely consistent (in terms of both the structure of the system and the composition of the hydrothermal products) with our model with complex feeding.

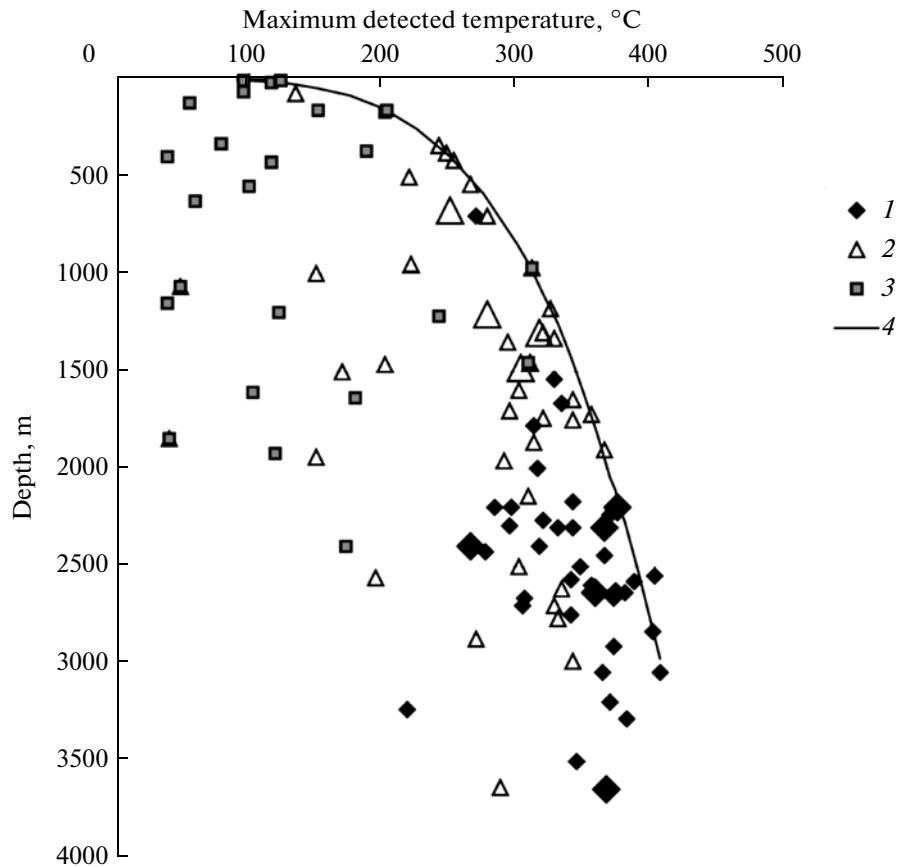


Fig. 21. Precipitation depths and temperatures of sulfide ores and native sulfur in oceanic hydrothermal systems (modified after [5]).

1—Hydrothermal systems with sulfide ores in mid-oceanic ridges, 2—hydrothermal systems with sulfide ores in island arcs, 3—hydrothermal systems with native sulfur in island arcs, 4—boiling curve of seawater. Large symbols show hydrothermal systems with ore masses greater than 300 thousand tons (according to [7]).

B) The SuSu Knolls group of hydrothermal vent fields, which was most thoroughly described in [73]. Massive precipitation of native sulfur was discovered at the flanks of North Su vent field, which are devoid of sulfide ores. The central part of the field does contain sulfide edifices with black smokers but no native sulfur. The nearby Suzette ore field (which is referred to as Solwara 1 starting in 2007) host a very large sulfide deposit, but no native sulfur has ever been found there.

C) The PACMANUS ore field comprises six hydrothermal areas, five of which contain sulfide ores and one (Snowcap) bears native sulfur and anhydrite but no sulfide edifices [75].

In all of the three examples, native sulfur and sulfides are precipitated separately in time and/or space.

Considered together with our simulations results, these facts led us to conclude that the occurrence of native sulfur is an indicator of the absence of submarine polymetallic sulfides.

Our simulation results indicate that an important distinctive feature of hydrothermal systems with mag-

matic feeding that precipitate native sulfur is the high acidity of the hydrothermal solutions (up to $\text{pH} < 1$), and this suppresses the precipitation of ore sulfides. Natural observations confirm that native sulfur is precipitated by more acidic hydrothermal springs. For example, pH values as low as 0.9 were detected at the North Su hydrothermal field in the East Manus Basin. It is important to emphasize that the concentrations of metals in the discharged hydrothermal solutions are high. Data in [73] indicate that the concentrations of Fe, Cu, Zn, Pb, and other metals in the solutions of sulfur-depositing hydrothermal springs at the Snowcap (PACMANUS field) and North Su (SuSu Knolls) areas are no lower than in hydrothermal springs at nearby portions of these fields where sulfide ores are precipitated.

6. Our simulation results indicate that a limited (no more than a few percent) involvement of magmatic fluids in the feeding of a hydrothermal solution enhances the precipitation of sulfides.

This implication of our model simulations can be confirmed if the contribution of a magmatic component to hydrothermal solutions is evaluated quantitatively. The only technique now making possible such an estimate is the hydrogen and oxygen isotopic composition of the water of hydrothermal solutions. Thereby solution samples should be selected that enable a reliable extrapolation of the analytical results to the end member. As of now, we are aware of only a single publication presenting such data [74], which were obtained on the PACMANUS field. According to these results, parts of the field with large sulfide edifices (up to 15–20 m high) are fed with solutions with up to a few percent magmatic component (author's estimates). The only part of the field with close to 20% magmatic component is the aforementioned Snowcap, at which native sulfur is precipitated but which is devoid of sulfide edifices.

It should also be mentioned that the Suzette (Solwara 1) ore field, whose sulfide accumulation has reserves of more than two million tons (data of Nautilus) [11] has, judging from its qualitative geochemical parameters, feeding with a magmatic component [73].

7. The summarizing data presented in Fig. 21 indicate that sulfide ore mineralization in island arcs is produced at generally lower seawater depths than in MOR. This difference is, however, not of causal but of correlation nature: the calderas of submarine volcanoes that are most productive in terms of base-metal sulfides occur in island arcs at higher levels than those of the axial valleys of mid-oceanic ridges.

The shallowest depths at which sulfide ores are formed in mid-oceanic ridges were detected at Axial Seamount (1540 m), S. Explorer (1850 m), and Lucky Strike (1618–1730 m). The absence of shallower depth sulfide accumulations at such hydrothermal systems as Grimsey (400 m), Menez Gwen (847–871 m), and Lost City (700–800 m) still cannot be unambiguously explained. The possible reasons for this can be (a) boiling (according to [6, 59, 60, and others], see above); (b) certain features of heat and material transfer, for example, the conditions of heat sink from the circulating water (see, for example, [76]); and (c) perhaps, also the scarcity of the observation statistics.

Our simulation showed that boiling is not such a strict constraint of depth of sulfide precipitation as was thought previously. Recent prospecting works in island arcs are of certain interest from this viewpoint.

One of the largest (according to provisional evaluations) bodies of base metal sulfide orebodies, the Hakurei body in the Bayonnaise caldera, Izu-Bonin arc, sits at a depth of 680–800 m [10]. The Black Forest hydrothermal fields found in 2004 at E. Diamante submarine volcano in the Mariana arc at a depth of 345 m host numerous sulfate–sulfide vents [13]. The three hydrothermal areas discovered somewhat later at

a submarine volcano at 24°48' S in the Tonga arc host active smokers and sulfide vents at depths of 540, 420, and 385 m [77, 78]. Finally, an active hydrothermal field with sulfide vents was lately discovered in the caldera of Kolumbo submarine volcano in the Aegean Sea at a depth of 505 m [79].

All of these finds, which are consistent with our simulation results, show that current hypotheses about low productivity of shallow-depth hydrothermal systems in terms of base-metal sulfide ore mineralization should be revised.

The comparison of the results of the thermodynamic simulation of hydrothermal systems in island arcs with results of natural observations (see above) generally make it possible to conclude that our model is in good agreement with of a broad spectrum of parameters with those of natural systems.

CONCLUSIONS

1. Ore-forming elements are more efficiently extracted by heated seawater from arc magmatic rocks than from MOR rocks, and this results in a rapid chemical evolution of the interiors of arc hydrothermal systems and their high productivity in terms of ore metals.

2. The metallogeny of arc mineral deposits is largely controlled by the abundances of metals in the predominant types of the host rocks of the hydrothermal systems. Sulfide ores in island arcs are likely relatively enriched in Cu, Pb, As, and Sb and are also richer in Zn, Pb, As, and Sb when formed at shallow seawater depths.

3. The occurrence of calcareous sedimentary rocks in the crustal sequences is favorable for the partial precipitation of ore metals in these rocks and thus decreases the productivity of the hydrothermal systems in terms of the generation of massive hydrothermal–sedimentary orebodies.

4. Convective systems in island arcs are likely too deficient in sulfide sulfur to effectively precipitate all scavenged metals. In this situation, the addition of minor amounts (close to 1%) of magmatic fluid as a supplier of sulfide sulfur should significantly enhance the ore-generating potential of the hydrothermal systems. This factor is the most significant for hydrothermal systems developing in acid rocks.

5. If much magmatic fluids generated during near-surface degassing (at pressures lower than 200 bars) come to hydrothermal systems, the latter actively precipitate sulfide sulfur and yield extremely acidic solutions in the ore-precipitation zones; these solutions hamper the crystallization of base-metal sulfides. The occurrence of significant amounts of native sulfur should be considered a negative exploration guide

when the ore-generating potential of hydrothermal systems is evaluated.

6. Boiling enhances the transport capacity of hydrothermal fluids with respect to chalcophile metals because H₂S is redistributed into the vapor phase. Boiling is not such a strict constraining factor of the ore-precipitation process as was thought previously. Zn and Pb can be transported in boiling fluids up to temperatures close to 200°C, which corresponds to seawater depths as shallow as 150–200 m. This widens the spectrum of areas promising in exploration for sulfide ores in island arcs.

ACKNOWLEDGMENTS

This study was supported by the Russian Foundation for Basic Research, project nos. 05-05-64223, 08-05-00306, and 11-05-00033.

REFERENCES

1. D. V. Grichuk, "Thermodynamic Models of Submarine Hydrothermal Systems," *Geochem. Int.* **42** (Suppl. 2), (2004).
2. Yu. V. Shvarov, "HCh: New Potentialities for the Thermodynamic Simulation of Geochemical Systems Offered by Windows," *Geochem. Int.* **46** (8), 834–839 (2008).
3. Y. A. Taran, J. W. Hedenquist, M. A. Korzhinsky, S. I. Tkachenko, K. I. Shmulovich, "Geochemistry of Magmatic Gases from Kudryavy Volcano, Iturup, Kuril Islands," *Geochim. Cosmochim. Acta* **59** (9), (1749–1761).
4. D. V. Grichuk, E. E. Abramova, and A. V. Tutubalin, "A Thermodynamic Model of a Submarine Massive Sulfide Formation in a Convecting Hydrothermal System," *Geol. Ore Dep.* **40** (1), 1–15 (1998).
5. InterRidge Vents Database. <http://www.interridge.org/irvents/>
6. Yu. A. Bogdanov, A. P. Lisitsyn, A. M. Sagalevich, and E. G. Gurvich, *Hydrothermal Ocean Floor Ore Formation* (Nauka, Moscow, 2006) [in Russian].
7. M. Hannington, J. Jamieson, T. Monecke, S. Petersen, S. Beaulieu, "The Abundance of Seafloor Massive Sulfide Deposits," *GSA Data Repository* 2011342, (2011).
8. G. P. Glasby and K. Notsu, "Submarine Hydrothermal Mineralization in the Okinawa Trough, SW of Japan: An Overview," *Ore Geol. Rev.* **23** (3–4), 299–339 (2003).
9. K. Iizasa, J. -I. Ishibashi, Y. Fujiwara, J. Hashimoto, Y. Horii, O. Ishizuka, S. Koyama, M. Yuasa, "Active Hydrothermal Field Associated with Black Smoker in the Myojin Knoll, Izu-Ogasawara Arc, Northwestern Pacific," *JAMSTEC J. Deep Sea Res.*, No. 14, 223–236 (1999).
10. K. Iizasa, M. Sasaki, K. Matsumoto, S. Shiokawa, M. Tanahashi, and On-Board Scientists, "A First Extensive Hydrothermal Field Associated with Kuroko-Type Deposit in a Silicic Submarine Caldera in a Nascent Rift Zone, Izu-Ogasawara (Bonin) Arc, Japan," in *Proceedings of Oceans'04 MTS/IEEE Techno-Ocean '04 Conference, Kobe, Japan, 2004* (Kobe, 2004), Vol. 2, 991–996.
11. Nautilus News Release 25.11.2011 (<http://www.nautilusminerals.com/s/Media-NewsReleases.asp?ReportID=492567>)
12. C. E. J. de Ronde, M. D. Hannington, P. Stoffers, I. C. Wright, R. G. Ditchburn, A. G. Reyes, E. T. Baker, G. J. Massoth, J. E. Lupton, S. L. Walker, R. R. Greene, C. W. R. Soong, J. Ishibashi, G. T. Lebon, C. J. Bray, and J. A. Resing, "Evolution of a Submarine Magmatic-Hydrothermal System: Brothers Volcano, Southern Kermadec Arc, New Zealand," *Econ. Geol.* **100** (6), 1097–1133 (2005).
13. R. W. Embley, E. T. Baker, D. A. Butterfield, W. W., Jr., Chadwick, J. E. Lupton, J. A. Resing, C. E. J. de Ronde, K. Nakamura, V. Tunnicliffe, J. F. Dower, S. G. Merle, "Exploring Submarine Ring of Fire," *Oceanography* **20** (4), 68–79 (2007).
14. E. T. Baker, R. W. Embley, S. L. Walker, J. A. Resing, J. E. Lupton, K. Nakamura, C. E. J. de Ronde, G. J. Massoth, "Hydrothermal Activity and Volcano Distribution along the Mariana Arc," *J. Geophys. Res.* **113** (B08), 09, 16 (2008).
15. P. R. Craddock and W. Bach, "Insights to Magmatic-Hydrothermal Processes in the Manus Back-Arc Basin as Recorded by Anhydrite," *Geochim. Cosmochim. Acta* **74** (19), 5514–5536 (2010).
16. C. E. J. de Ronde, G. J. Massoth, E. T. Baker, and J. E. Lupton, "Submarine Hydrothermal Venting Related to Volcanic Arcs," in *Giggenbach Memorial Volume*, Ed. by S. F. Simmons and I. J. Graham, *Soc. Econ. Geol.*, Sp. Publ. **10**, 91–110 (2003).
17. I. I. Smirnov, *Plutonism and Neptunism in the Evolution of the Study of Mineral Deposits* (Nauka, Moscow, 1987) [in Russian].
18. S. G. Krasnov, Hydrothermal Activity and Sulfide Ore-formation in the Ocean Doctoral Dissertation in Geology and Mineralogy (VNIIOkeangeologiya, St. Petersburg, 1993) [in Russian].
19. D. V. Grichuk, *Thermodynamic Models of Submarine Hydrothermal Systems* (Nauchnyi mir, Moscow, 2000) [in Russian].
20. K. Yang and S. D. Scott, "Possible Contribution of a Metal-Rich Magmatic Fluid to a Sea-Floor Hydrothermal System," *Nature* **383** (6599), 420–423 (1996).
21. K. Yang and S. D. Scott, "Magmatic Degassing of Volatiles and Ore Metals into a Hydrothermal System on the Modern Sea Floor of the Eastern Manus Back-Arc Basin, Western Pacific," *Econ. Geol.* **97** (5), 1079–1100 (2002).
22. K. Yang and S. D. Scott, "Vigorous Exsolution of Volatiles in the Magma Chamber Beneath a Hydrothermal System on the Modern Sea Floor of the Eastern Manus Back-Arc Basin, Western Pacific: Evidence from Melt Inclusions," *Econ. Geol.* **100** (6), 1085–1096 (2005).
23. T. Gamo, K. Okamura, J. -L. Charlou, T. Urabe, J. -M. Auzende, J. Ishibashi, K. Shitashima, H. Chiba, R. A. Binns, K. Gena, K. Henry, O. Matsubayashi, R. Moss, Y. Nagaya, J. Naka, E. Ruellan, "Acidic and Sulfate-Rich Hydrothermal Fluids from the Manus Back-Arc Basin, Papua New Guinea," *Geology* **25** (2), 139–142 (1997).
24. P. M. Herzig, M. D. Hannington, and A. J. Arribas, "Sulfur Isotopic Composition of Hydrothermal Precipitates from the Lau Back-Arc: Implication for Magmatic Contributions to Seafloor Hydrothermal Systems," *Miner. Deposita* **33** (3), 226–237 (1998).

25. J. Seewald, E. Reeves, P. Saccoccia, O. Rouxel, E. Walsh, R. Price, M. Tivey, W. Bach, M. Tivey, "and Scientific MGLN06MV. "Water-Rock Reaction, Substrate Composition, Magmatic Degassing, and Mixing as Major Factors Controlling Vent Fluid Compositions in Manus Basin Hydrothermal Systems," *Eos Trans. Am. Geophys. Union* **87** (52), No. B34A-02 (2006).
26. D. A. Butterfield, K. K. Roe, S. A. Bolton, J. A. Baross, J. E. Lupton, M. D. Lilley, R. W. Embley, W. W. Chadwick, J. A. Resing, "Overview of Vent Fluid Chemistry from the Marianas Volcanic Arc," *Eos Trans. Am. Geophys. Union* **85** (47), No. V44A-01 (2004).
27. K. Takai, T. Nakagawa, Y. Suzuki, H. Hirayama, A. Kosaka, U. Tsunogai, T. Gamo, K. H. Nealson, K. Horikoshi, "Geomicrobiological Exploration and Characterization of Novel Deep-Sea Hydrothermal Activities Accompanying with Extremely Acidic White Smokers and Elemental Sulfur Chimneys at the TOTO Caldera in the Mariana Volcanic Arc," *Eos Trans. Am. Geophys. Union* **85** (47), V54A-06 (2004).
28. C. E. J. de Ronde, G. J. Massoth, D. A. Butterfield, B. W. Christenson, J. Ishibashi, R. G. Ditchburn, M. D. Hannington, R. L. Brathwaite, J. E. Lupton, V. S. Kamenetsky, I. J. Graham, G. F. Zellmer, R. P. Dziak, R. W. Embley, V. M. Dekov, F. Munnik, J. Lahr, L. J. Evans, K. Takai, "Submarine Hydrothermal Activity and Gold-Rich Mineralization at Brothers Volcano, Kermadec Arc, New Zealand," *Miner. Deposita* **46** (5–6), 541–584 (2011).
29. S. Petersen, P. M. Herzig, U. Schwarz-Schampera, M. D. Hannington, I. R. Jonasson, "Hydrothermal Precipitates Associated with Bimodal Volcanism in the Central Bransfield Strait, Antarctica," *Miner. Deposita* **39** (3), 358–379 (2004).
30. A. B. Ronov, A. A. Yaroshevskii, and A. A. Migdisov, *Chemical Structure of the Earth's Crust and the Geochemical Balance of Major Elements*, (Nauka, Moscow, 1990).
31. *Guidebook on Geochemical Exploration of Mineral Resources* Ed. by A. P. Solovov, A. Ya. Arkhipov, et al. (Nedra, Moscow, 1990) [in Russian].
32. M. A. Korzhinskii, S. I. Tkachenko, R. F. Bulgakov, and K. I. Shmulovich, "Condensate Compositions and Native Metals in Sublimates of High-Temperature Gas Streams of Kudryavyi Volcano, Iturup Island, Kuril Islands," *Geochem. Int.* **34** (12), 1057–1064 (1996).
33. S. I. Tkachenko, Extended Abstracts of Candidate's Dissertation in Geology and Mineralogy (IEM RAN, Chernogolovka, 1996) [in Russian].
34. T. P. Fischer, W. F. Giggenbach, Y. Sano, and S. N. Williams, "Fluxes and Sources of Volatiles Discharged from Kudryavy, a Subduction Zone Volcano, Kurile Islands," *Earth Planet. Sci. Lett.* **160** (1–2), 81–96 (1998).
35. M. A. Yudovskaya, V. V. Distler, I. V. Chaplygin, A. V. Mokhov, N. V. Trubkin, S. A. Gorbacheva, "Gaseous Transport and Deposition of Gold in Magmatic Fluid: Evidence from the Active Kudryavy Volcano, Kurile Islands," *Miner. Deposita* **40** (8), 828–848 (2006).
36. R. B. Symonds, M. H. Reed, and W. I. Rose, "Origin, Speciation and Fluxes of Trace Element Gases at Augustine Volcano, Alaska: Insights into Magma Degassing and Fumarolic Processes," *Geochim. Cosmochim. Acta* **56** (2), 633–657 (1992).
37. R. B. Symonds and M. H. Reed, "Calculation of Multi-component Chemical Equilibria in Gas–Solid–Liquid Systems: Calculation Methods, Thermochemical Data and Applications to Studies of High-Temperature Volcanic Gases with Examples from Mount St. Helens," *Am. J. Sci.* **293** (8), 758–864 (1993).
38. *Great Fissure Tolbachik Eruption. Kamchatka 1975–1976*, Ed. by S. A. Fedotov (Nauka, Moscow, 1984) [in Russian].
39. I. A. Menyailov, L. P. Nikitina, V. N. Shapar', A. M. Rozhkov, A. Z. Miklishanskii, "Chemical Composition and Content of Metals in Gas Emanations from the Alaid Volcano Crater during 1981 Eruption," *Vulkanol. Seismol.*, No. 1, 26–31 (1986).
40. L. P. Nikitina, I. A. Menyailov, V. N. Shapar', and L. N. Gartseva, "Geochemistry and Analytical Chemistry of the Fumarole Gases of Ebeko Volcano, Paramushir Island," *Vulkanol. Seismol.*, No. 1, 62–72 (1989).
41. R. B. Symonds, W. I. Rose, M. H. Reed, F. E. Lichte, D. L. Finnegan, "Volatilisation, Transport and Sublimation of Metallic Elements in High-Temperature Gases at Merapi Volcano, Indonesia," *Geochim. Cosmochim. Acta* **51** (8), 2083–2101 (1987).
42. J. B. Gemell, "Geochemistry of Metallic Trace Elements in Fumarolic Condensates from Nicaraguan and Costa Rican Volcanoes," *J. Volcanol. Geotherm. Res.* **33** (1–3), 161–181 (1987).
42. I. A. Menyailov, L. P. Nikitina, V. N. Shapar, and V. P. Pilipenko, "Temperature Increase and Chemical Change of Fumarolic Gases at Momotombo Volcano, Nicaragua, in 1982–1985: Are These Indicators of a Possible Eruption?," *J. Geophys. Res.* **91** (B12), 12199–12214 (1986).
43. J. P. Quisefit, J. P. Toutain, G. Bergametti, M. Javoy, B. Cheynet, A. Person, "Evolution versus Cooling of Gaseous Volcanic Emissions from Momotombo Volcano, Nicaragua: Thermochemical Model and Observations," *Geochim. Cosmochim. Acta* **53** (10), 2591–2608 (1989).
44. K. L. von Damm, "Seafloor Hydrothermal Activity: Black Smoker Chemistry and Chimneys," *Ann. Rev. Earth Planet. Sci. Lett.* **18**, 173–204 (1990).
45. P. J. Wallace and I. S. E. Carmichael, "S Speciation in Submarine Basaltic Glasses as Determined by Measurements of SK α X-Ray Wavelength Shifts," *Am. Mineral.* **79** (1/2), 161–167 (1994).
46. D.-Y. Peng and D. B. Robinson, "A New Two-Constant Equation of State," *Industr. Eng. Chem. Fundam.* **15** (1), 59–64 (1976).
47. R. Stryjek and J. H. Vera, "PRSV2: A Cubic Equation of State for Accurate Vapor–Liquid Equilibria Calculations," *Can. J. Chem. Engin.* **64** (10), 820–826 (1986).
48. K. Nilsson and C. L. Peach, "Sulfur Speciation, Oxidation State, and Sulfur Concentration in Backarc Magmas," *Geochim. Cosmochim. Acta* **57** (15), 3807–3813 (1993).
49. N. N. Akiniev and A. V. Zotov, "Thermodynamic Description of Chloride, Hydrosulfide, and Hydroxo Complexes of Ag(I), Cu(I), and Au(I) at Temperatures of 25–500°C and Pressures of 1–2000 bars," *Geochem. Int.* **39** (10), 990–1006 (2001).
50. W. Liu and D. C. McPhail, "Thermodynamic Properties of Copper Chloride Complexes and Copper Transport in Magmatic–Hydrothermal Solutions," *Chem. Geol.* **221** (1–2), 21–39 (2005).
51. G. S. Pokrovski, S. Kara, and J. Roux, "Stability and Solubility of Arsenopyrite, FeAsS, in Crustal Fluids,"

- Geochim. Cosmochim. Acta **66** (13), 2361–2378 (2002).
52. A. V. Zotov, N. D. Shikina, and N. N. Akinfiev, “Thermodynamic Properties of the Sb(III) Hydroxide Complex $\text{Sb}(\text{OH})_3(\text{Aq})$ at Hydrothermal Conditions,” *Geochim. Cosmochim. Acta* **67** (10) (1821–1836).
 53. B. Bessinger and J. A. Apps, *The Hydrothermal Chemistry of Gold, Arsenic, Antimony, Mercury and Silver* (Lawrence Berkley National Laboratory, Berkeley, 2005).
 54. Yu. V. Shvarov, “Algorithmization of the Numeric Equilibrium Modeling of Dynamic Geochemical Processes,” *Geochem. Int.* **37** (6), 571–576 (1999).
 55. *Sulfide Deposits around the World*, Ed. by V. I. Smirnov (Nedra, Moscow, 1979) [in Russian].
 56. M. V. Borisov, *Geochemical and Thermodynamic Models of Veined Hydrothermal Ore Formation* (Nauchnyi mir, Moscow, 2000) [in Russian].
 57. S. G. Krasnov and T. V. Stepanova, “The Formation of a Large Oceanic Massive Sulfide Ore Body (Middle Valley, Endeavor Ridge): Evidence from Geochemical Study of the Cores,” *Geochem. Int.* **34** (9), 768–789 (1996).
 58. G. A. Karpov, *Modern Hydrothermal Springs and Mercury–Antimony–Arsenic Mineralization* (Nauka, Moscow, 1988) [in Russian].
 59. J. D. Ridge, “Volcanic Exhalations and Ore Deposition in the Vicinity of the Seafloor,” *Miner. Deposita* **8** (4), 332–348 (1973).
 60. G. P. Glasby, G. A. Cherkashov, G. M. Gavrilenko, V. A. Rashidov, I. B. Slotsov, “Submarine Hydrothermal Activity and Mineralization on the Kurile and Western Aleutian Island Arcs, N.W. Pacific,” *Mar. Geol.* **231** (1–4), 163–180 (2006).
 60. S. G. Krasnov, “Minimum Depths of the Formation of Massive Sulfide Ores on the Ocean Floor,” *Dokl. Akad. Nauk SSSR* **296** (5), 1188–1191 (1987).
 61. M. Hannington, P. Herzig, S. Scott, G. Thompson, P. Rona, “Comparative Mineralogy and Geochemistry of Gold-Bearing Sulfide Deposits on the Mid-Ocean Ridges,” *Mar. Geol.* **101** (1/4), 217–248 (1991).
 62. P. Halbach, B. Pracejus, and A. Maerten, “Geology and Mineralogy of Massive Sulfide Ores from the Central Okinawa Trough, Japan,” *Econ. Geol.* **88** (8), 2206–2221 (1993).
 63. M. Ito, T. Noguchi, J. Takada, and T. Oomori, “Geochemical Characteristics of Sulfide Chimneys Collected from Arc-Backarc Hydrothermal Fields at Western Pacific,” *Geochim. Cosmochim. Acta* **70** (18), A281 (2006).
 64. A. G. Reyes, G. Massoth, C. de Ronde, and I. S. Wright, “Hydrothermal Mineralization in Arc-Type Submarine Volcanoes,” *Geochim. Cosmochim. Acta* **71** (18), A528 (2007).
 65. A. I. Krivtsov, O. V. Minina, A. G. Volchkov, E. E. Abramova, D. V. Grichuk, E. A. El’yanova, *Sulfide Deposits. Series: Noble and Base Metal Deposits* (TsNIGRI, Moscow, 2002) [in Russian].
 66. P. M. Herzig, S. E. Humphris, D. J. Miller, and R. A. Zierenberg, *Proc. Ocean Drill. Progr., Sci. Res.* **158**, (1998).
 67. N. C. White and J. W. Hedenquist, “Epithermal Environments and Style of Mineralization: Variations and Their Causes, and Guidelines for Exploration,” *J. Geochem. Explor.* **36** (1–3), 445–474 (1990).
 68. K. Gena, T. Mizuta, D. Ishiyama, and T. Urabe, “Acid-Sulphate Type Alteration and Mineralization in the Desmos Caldera, Manus Back-Arc Basin, Papua New Guinea,” *Resour. Geol.* **51** (1), 31–44 (2001).
 69. K. S. Lackschewitz, C. W. Devey, P. Stoffers, R. Botz, A. Eisenhauer, M. Kummert, M. Schmidt, A. Singer, “Mineralogical, Geochemical and Isotopic Characteristics of Hydrothermal Alteration Processes in the Active, Submarine, Felsic-Hosted PACMANUS Field, Manus Basin, Papua New Guinea,” *Geochim. Cosmochim. Acta* **68** (21), 4405–4427 (2004).
 71. R. W. Embley, W. W., Jr. Chadwick, E. T. Baker, D. A. Butterfield, J. A. Resing, C. E. J. de Ronde, V. Tunnicliffe, J. E. Lupton, S. K. Juniper, K. H. Rubin, R. J. Stern, G. T. Lebon, K. -I. Nakamura, S. G. Merle, J. R. Hein, D. A. Wiens, Y. Tamura, “Long-Term Eruptive Activity at a Submarine Arc Volcano,” *Nature* **441** (7092), 494–497 (2006).
 72. D. Stuben, S. H. Bloomer, N. E. Taibi, Th. Neumann, V. Bendel, U. Puschel, A. Barone, A. Lange, W. Shiyang, L. Cuizhong, Z. Deyu, “First Results of Study of Sulphur-Rich Hydrothermal Activity from an Island-Arc Environment: Esmeralda Bank in the Mariana Arc,” *Mar. Geol.* **103** (1–3), 521–528 (1992).
 73. P. R. Craddock, *Geochemical Tracers of Processes Affecting the Formation of Seafloor Hydrothermal Fluids and Deposits in the Manus Back-Arc Basin*, Ph.D. Thesis, MIT/WHOI (2009).
 74. E. Reeves, *Laboratory and Field-Based Investigations of Subsurface Geochemical Processes in Seafloor Hydrothermal Systems. Ph. D. Thesis, Massachusetts Institute of Technology* (Oceanographic Institution, Woods Hole, 2010).
 75. M. Tivey, W. Bach, M. Tivey, J. Seewald, P. Craddock, O. Rouxel, D. Yoerger, C. Yeats, T. McConachy, M. Quigley, D. Vanko, and Science Party of MGLN06MV, “Investigating the Influence of Magmatic Volatile Input and Seawater Entrainment on Vent Deposit Morphology and Composition in Manus Basin (Back-Arc) Hydrothermal Systems,” *Eos Trans. Am. Geophys. Union* **87** (52), B34A-01 (2006).
 76. T. E. Jupp and A. Schultz, “The Physical Balances in Subseafloor Hydrothermal Convection Cells,” *J. Geophys. Res.* **109** (B05101), 12 (2004).
 77. P. Stoffers, T. J. Worthington, M. D. Hannington, U. Schwarz-Schampera, G. J. Massoth, L. J. Lundsten, “Submarine Volcanoes and High-Temperature Hydrothermal Venting on the Tonga Arc, SW Pacific,” *Eos Trans. Am. Geophys. Union* **86** (52), V51C-1494 (2005).
 78. P. Stoffers, T. J. Worthington, U. Schwarz-Schampera, M. D. Hannington, G. J. Massoth, R. Hekinian, M. Schmidt, L. J. Lundsten, L. J. Evans, R. Vainomou’unga, T. Kerby, “Submarine Volcanoes and High-Temperature Hydrothermal Venting on the Tonga Arc, Southwest Pacific,” *Geology* **34** (6), 453–456 (2006).
 79. H. Sigurdsson, S. Carey, M. Alexandri, G. Vougioukalakis, K. Croff, C. Roman, D. Sakellariou, C. Anagnostou, G. Rousakis, C. Ioakim, A. Gogou, D. Ballas, T. Misaridis, P. Nomikou, “High-Temperature Hydrothermal Vent Field of Kolumbo Submarine Volcano, Aegean Sea: Site of Active Kuroko-Type Mineralization,” *Eos Trans. Am. Geophys. Union* **87** (52), OS34A-03 (2006).